Supporting Information: Benchmarking Various Nonadiabatic Semiclassical Mapping Dynamics Methods with Tensor-Train Thermo-Field Dynamics

Zengkui Liu[#],[1,2,3] Ningyi Lyu[#],[4,1] Zhubin Hu,[1,2,5] Hao Zeng,[1,2,5] Victor S. Batista,[4] and Xiang Sun[1,2,3,5,a)]

[1)]*Division of Arts and Sciences, NYU Shanghai, 567 West Yangsi Road, Shanghai 200124, China*

[2)]*NYU-ECNU Center for Computational Chemistry at NYU Shanghai, 3663 Zhongshan Road North, Shanghai 200062, China*

[3)]*Department of Chemistry, New York University, New York, New York 10003, United States*

[4)]*Department of Chemistry, Yale University, P.O. Box 208107, New Haven, Connecticut 06520-8107, United States*

[5)]*State Key Laboratory of Precision Spectroscopy, East China Normal University, Shanghai 200062, China*

I. MODEL PARAMETERS

A. Spin-Boson Model Bath Modes

The bath modes in the spin-boson models tested in this work are described by Ohmic spectral density

$$J(\omega) = \frac{1}{2}\pi\hbar\xi\,\omega e^{-\omega/\omega_c}, \tag{S1}$$

and it is discretized using Makri's approach[1]. The frequencies and electronic-vibronic couplings are given by

$$\omega_j = \omega_c \ln(1 - j\omega_0/\omega_c), \quad (j = 1, \cdots, N), \tag{S2}$$

$$c_j = \omega_j \sqrt{\xi\hbar\omega_0}, \tag{S3}$$

where

$$\omega_0 = \frac{\omega_c}{N}\left(1 - e^{-\omega_{\max}/\omega_c}\right), \tag{S4}$$

where ω_c is the characteristic frequency of the bath, ξ serves as Kondo parameter of the bath, and ω_{max} sets a maximum frequency for discretized bath modes.

B. LVC Model Parameters

The three LVC models are adopted from Ref. 2, and the following parameters are converted to be directly used in our expression in atomic units.

1. Fulvene

The model contains 2 states and 30 nuclear modes. The vertical shift of PES of 2 states are given by $\varepsilon_0 = 0$ and $\varepsilon_1 = 1.8764 \times 10^{-1}$. Initial electronic state is $|1\rangle$ and initial nuclear state is on the PES of $|0\rangle$, where initial position shift of the kth nuclear mode, S_k, is given by

$$S_k = 0. \tag{S5}$$

Indexes of the kth nuclear mode, k, frequencies the kth nuclear mode, ω_k, nuclear-electronic coupling between $|1\rangle$ and the kth nuclear mode, g_k, and electronic state coupling between $|0\rangle$ and $|1\rangle$, $\gamma_{01,k}$ are given in the list below.

[a)]Electronic mail: xiang.sun@nyu.edu

TABLE S1. Categorization of the spin-boson models #1–9 characterized by parameters including electronic coupling Γ, reaction free energy $-\Delta E$, reorganization energy E_r and cutoff frequency ω_c of nuclear modes. Models #1–#4 and #9 are given in the reduced unit, and Models #5–#8 are given with energy unit in cm^{-1}. Here, we use $\omega_c/\Gamma < 1$ to determine the adiabatic regime, whereas $\omega_c/\Gamma > 1$ for nonadiabatic regime. For comparison, we also show the adiabatic parameter[3] $\gamma_{\mathrm{adia}} = \frac{|\Gamma|^2}{2\hbar\omega_c}\sqrt{\frac{\pi}{E_r k_B T}}$, where $\gamma_{\mathrm{adia}} \gg 1$ is the adiabatic limit and $\gamma_{\mathrm{adia}} \ll 1$ is the nonadiabatic limit. When in the Marcus weak-coupling nonadiabatic limit, we further categorize models into the normal region ($-\Delta E < E_r$) and the inverted region ($-\Delta E > E_r$).

model #	temperature	Γ	$-\Delta E$	E_r	ω_c	E_r/Γ	ω_c/Γ	γ_{adia}	regime	Marcus
1	0	1.0	2.0	0.198	1.0	0.198	1.0	∞	intermediate	–
1	$0.2\ \Gamma/k_B$	1.0	2.0	0.198	1.0	0.198	1.0	4.45	intermediate	–
1	$2\ \Gamma/k_B$	1.0	2.0	0.198	1.0	0.198	1.0	1.40	intermediate	–
2	0	1.0	2.0	0.397	2.0	0.397	2.0	∞	nonadiabatic	inverted
2	$0.2\ \Gamma/k_B$	1.0	2.0	0.397	2.0	0.397	2.0	1.57	nonadiabatic	"
3	$0\ \Gamma/k_B$	1.0	2.0	1.488	7.5	1.488	7.5	∞	nonadiabatic	inverted
3	$0.2\ \Gamma/k_B$	1.0	2.0	1.488	7.5	1.488	7.5	0.22	nonadiabatic	"
3	$2\ \Gamma/k_B$	1.0	2.0	1.488	7.5	1.488	7.5	0.07	nonadiabatic	"
3	$10\ \Gamma/k_B$	1.0	2.0	1.488	7.5	1.488	7.5	0.03	nonadiabatic	"
4	0	1.0	0	0.992	2.5	0.992	2.5	∞	nonadiabatic	normal
4	$0.2\ \Gamma/k_B$	1.0	0	0.992	2.5	0.992	2.5	0.80	nonadiabatic	"
5	0	20	100	39.73	53	1.99	2.65	∞	nonadiabatic	inverted
5	300 K	20	100	39.73	53	1.99	2.65	0.07	nonadiabatic	"
6	0	20	100	119.2	53	5.96	2.65	∞	nonadiabatic	normal
6	300 K	20	100	119.2	53	5.96	2.65	0.04	nonadiabatic	"
7	0	100	100	79.46	53	0.79	0.53	∞	adiabatic	–
7	300 K	100	100	79.46	53	0.79	0.53	1.30	adiabatic	–
8	0	100	100	198.6	53	1.99	0.53	∞	adiabatic	–
8	300 K	100	100	198.6	53	1.99	0.53	0.82	adiabatic	–
9	$0\ \Gamma/k_B$	1.0	2.0	0.080	0.5	0.080	0.5	∞	adiabatic	–
9	$0.2\ \Gamma/k_B$	1.0	2.0	0.080	0.5	0.080	0.5	14.0	adiabatic	–
9	$2\ \Gamma/k_B$	1.0	2.0	0.080	0.5	0.080	0.5	4.43	adiabatic	–
9	$10\ \Gamma/k_B$	1.0	2.0	0.080	0.5	0.080	0.5	1.98	adiabatic	–

TABLE S2: LVC model parameters of Fulvene: mode frequencies, electronic-vibrational coupling coefficients, diabatic coupling coefficients.

index(j)	ω_j	g_j	γ_j
0	0.00098662	0.0	0.0
1	0.0017237	-4.017022442567691e-10	-9.251752168898602e-06
2	0.002419	0.0	0.0
3	0.0028634	0.0	0.0
4	0.0033546	0.0003759979723393518	-2.089250879297745e-10
5	0.0034833	0.0	0.0
6	0.0036851	0.0	0.0
7	0.0038835	0.0	0.0
8	0.0043459	1.9401927757132537e-08	0.00043069102111004825
9	0.0041842	0.0	0.0
10	0.0043828	0.0	0.0
11	0.0044617	0.0	0.0
12	0.0046002	0.0004847504439334553	-1.0211019761047376e-08
13	0.0051482	2.8393289171684215e-09	0.0003741094959596722
14	0.005131	0.00046551553549655037	-2.15487533919227e-09
15	0.0057261	1.456364035352288e-07	4.573025446765293e-05
16	0.0057567	-0.0005673852835779995	9.77698448026384e-09
17	0.0067668	-5.3006238098764566e-08	0.0005158395298814855
18	0.007755	9.94137312122928e-09	0.000948609011089395
19	0.0072129	0.0006124639957956916	3.1798189650678066e-08
20	0.0076025	0.0004843969125114496	1.2354279278867303e-08
21	0.007927	-0.0016540681061758009	-2.0902442097475118e-09
22	0.0082881	6.370818365096599e-08	-0.0003500449651151977
23	0.0085797	0.0024292270480869424	-3.951453743284868e-09
24	0.016669	-0.0004744220261876972	2.0578600869225783e-10
25	0.017018	-6.168472785629357e-08	7.081644182465679e-06

26	0.017046	9.746328700336348e-05	-3.3802069665332627e-09
27	0.017134	-9.600371776653549e-08	-5.2329965080110655e-05
28	0.017176	-8.41033622422457e-05	1.0460726734688369e-08
29	0.017397	1.5356847769815912e-08	3.032459736114727e-06

2. BMA

The model contains 2 states and 78 nuclear modes. The vertical shift of PES of 2 states are given by $\varepsilon_0 = 0$ and $\varepsilon_1 = 2.9255 \times 10^{-2}$. The rest of the parameters are given in the file. Initial electronic state is $|0\rangle$ and initial nuclear distribution is on the PES of $|1\rangle$, where initial position shift of the kth nuclear mode, S_k, is given by

$$S_k = \frac{g_k}{\omega_k^2}. \tag{S6}$$

Indexes of the kth nuclear mode, k, frequencies the kth nuclear mode, ω_k, nuclear-electronic coupling between $|1\rangle$ and the kth nuclear mode, g_k, and electronic state coupling between $|0\rangle$ and $|1\rangle$, $\gamma_{01,k}$ are given in the list below.

TABLE S3: LVC model parameters of BMA: mode frequencies, electronic-vibrational coupling coefficients, diabatic coupling coefficients.

index(j)	ω_j	g_j	γ_j
0	0.00014364	1.1423613652937674e-09	-2.5410577098240018e-11
1	0.00070042	-1.6305363236315834e-10	-1.723562377479417e-11
2	0.0013609	7.918519669752042e-10	-4.0324872355024254e-07
3	0.0014446	5.133346152419492e-10	5.040986970201371e-10
4	0.0015662	-4.911287878143573e-10	-1.3560457626477803e-11
5	0.0017429	-4.067137153814572e-06	-3.9112081726965646e-11
6	0.0019084	3.2580450337219094e-09	-4.0491410047016637e-10
7	0.0019872	2.311682460428508e-09	-1.3374743787769545e-05
8	0.002068	8.952261259190328e-09	1.2770819513453316e-10
9	0.0021338	-3.6317455981340158e-06	-3.497462334708524e-10
10	0.0022608	1.2793230067613104e-09	9.407821679840664e-06
11	0.0029137	3.7104418251143215e-05	-3.0249663201298623e-10
12	0.0030567	1.4125938559083428e-09	-1.0566533766778964e-10
13	0.0031336	1.1090473758854489e-08	-5.015903546781736e-11
14	0.0035698	-5.176669174116422e-06	-5.410163589439787e-11
15	0.0035937	-3.314915636284474e-10	1.587469138731742e-05
16	0.0036504	-3.3888759198648745e-10	2.846982032803579e-10
17	0.003728	9.485259336465187e-09	7.996070567772647e-11
18	0.0039665	-4.45937289775076e-05	-2.997666466319844e-10
19	0.0042489	4.925858477779574e-10	7.696877940110523e-10
20	0.0043519	-1.1067607735346874e-10	1.1089377482933836e-10
21	0.0044641	4.663745293063977e-09	1.5250945540167663e-10
22	0.004502	7.682600178325046e-09	-1.2066043581381598e-10
23	0.0045767	-9.801322066154138e-05	1.9039108704291544e-10
24	0.0048162	7.692168229486403e-10	2.910518254929901e-07
25	0.0048881	1.5658850977491613e-09	-2.0579465040963773e-10
26	0.0049876	7.656233190777303e-09	1.5765865672070152e-05
27	0.0050317	-0.00017248427380590962	-2.091290245248325e-10
28	0.0050655	1.6415185287677993e-08	9.159878366823437e-11
29	0.0053204	8.93090486868156e-06	-3.316338784379907e-11
30	0.0053536	-3.955844093358585e-10	-5.517840943539275e-10
31	0.005511	1.3488701152816754e-09	2.2232230166458786e-10
32	0.0055488	1.3718127721860588e-09	1.8288850555338898e-11
33	0.005759	6.565608626269998e-09	-8.218678574442489e-11
34	0.0058294	3.5171624798502553e-09	-1.1027303802474113e-06
35	0.005913	3.290996450628897e-05	1.532768639898729e-11
36	0.0060599	3.3675124078096426e-09	-1.8925763808379305e-10
37	0.0061243	2.4884449251565124e-10	2.462619815863423e-10
38	0.0062667	-2.4184932661445847e-09	-2.1255920490081583e-05

39	0.0064994	-0.00020685992352148348	8.437569506122009e-11
40	0.0067154	0.0008734788736010733	-2.0387729520894178e-10
41	0.0067344	-4.150109765768804e-09	-1.6106581581259257e-05
42	0.0068892	5.557511670498839e-09	9.992515047140034e-13
43	0.0069729	3.326962070038611e-09	-1.6346721922362294e-10
44	0.0069762	-2.0296246790970985e-09	2.543128075273599e-10
45	0.007123	0.00025945592356645087	-4.0949845200195815e-11
46	0.0071467	2.8939101926598896e-09	-4.879457887652962e-10
47	0.007281	-4.454332760574136e-09	2.356951448461338e-05
48	0.0073408	-7.242400959814363e-09	5.3482213736369594e-11
49	0.0074179	3.3654215695344167e-09	6.097118969941918e-05
50	0.0074193	1.9879179409752557e-09	-2.975718233323461e-09
51	0.0074574	0.0004940699497194765	2.792501697879627e-10
52	0.0074792	1.373340006145601e-08	3.6201519305576114e-10
53	0.0075643	-4.298987641519373e-08	-3.839857257340434e-10
54	0.0075861	-0.0008294886119738209	-1.2599628565682403e-10
55	0.0078827	-0.00038333626259089035	1.0795315955259021e-10
56	0.0079413	0.00046363326196043893	-3.0784421616513274e-11
57	0.0081991	-8.608301097466235e-10	-2.112324315244797e-06
58	0.0082369	-4.636249430171591e-09	5.531026329632512e-10
59	0.0082473	2.8584818099552076e-09	2.6953787050282935e-10
60	0.0082744	1.9507171691611267e-05	2.1459253316707923e-10
61	0.008738	0.0011015361492606585	1.516014364282872e-11
62	0.016495	-7.156150628773475e-09	2.8676489391276613e-05
63	0.016496	-2.2625418736845518e-08	-3.488727572371337e-08
64	0.0165	1.3834315487222346e-08	4.76378295412375e-08
65	0.0165	2.8878651883354943e-06	-1.946823449622487e-08
66	0.016556	0.00012214268562092616	-3.941937822413743e-11
67	0.01659	-9.511267729080073e-05	6.068514423048692e-12
68	0.016717	-2.3597491391495413e-08	3.383888798960155e-11
69	0.016724	1.8491653442361502e-05	4.4465837608375266e-11
70	0.016779	1.8712449768974665e-10	-1.911789049842843e-11
71	0.016789	1.2989630453269253e-05	-8.222792400946835e-11
72	0.017025	3.892736844547805e-09	2.8006202195942238e-06
73	0.017032	2.864622170548849e-08	-1.3684933066230173e-09
74	0.017032	-6.2360018758695055e-09	4.45236674125032e-09
75	0.017038	1.2353199342243206e-05	1.0880954967501701e-09
76	0.017316	-1.1732588758223822e-08	-2.7965564859777105e-12
77	0.017437	1.7731571039837392e-11	2.5799779190969837e-11

3. MIA

The model contains 2 states and 96 nuclear modes. The vertical shift of PES of 2 states are given by $\varepsilon_0 = 0$ and $\varepsilon_1 = 2.4615 \times 10^{-3}$. The rest of the parameters are given in the file. Initial electronic state is $|0\rangle$ and initial nuclear configuration is taken on the PES of $|1\rangle$, where initial position shift of the kth nuclear mode, S_k, is given by

$$S_k = \frac{g_k}{\omega_k^2}. \tag{S7}$$

Indexes of the kth nuclear mode, k, frequencies the kth nuclear mode, ω_k, nuclear-electronic coupling between $|1\rangle$ and the kth nuclear mode, g_k, and electronic state coupling between $|0\rangle$ and $|1\rangle$, $\gamma_{01,k}$ are given in the list below.

TABLE S4: LVC model parameters of MIA: mode frequencies, electronic-vibrational coupling coefficients, diabatic coupling coefficients.

index(j)	ω_j	g_j	γ_j
0	3.2508e-05	-5.3058321491764895e-09	-4.310678597862522e-10
1	0.000178	1.1332943122631472e-07	-3.494715484957252e-06
2	0.00033693	1.3644674717153392e-09	2.3522769422253407e-10
3	0.00041833	4.151369182221331e-08	-1.8243975941516504e-10

4	0.00068418	-9.86374235439065e-08	4.5282712182235726e-06
5	0.0010397	7.064421072923811e-10	-4.2617396193725866e-09
6	0.0013946	-1.5283546067682066e-08	8.401730426396695e-10
7	0.0014123	1.1112201727201949e-05	-6.796823715315854e-10
8	0.0014261	1.6450640079730637e-07	2.0647324419431442e-07
9	0.001666	3.646723962651409e-09	-1.8216068648053564e-09
10	0.0018807	-1.5369278328926183e-08	-2.2500987756668593e-10
11	0.002059	6.257832461635578e-10	-8.930490948984832e-11
12	0.0020805	2.584449765451149e-07	9.215549153946279e-09
13	0.0021475	-1.3940801067827845e-07	1.4103921832906973e-05
14	0.0022491	-1.538171977731879e-08	-1.0002812898292159e-05
15	0.0022329	1.2105892429709177e-05	2.1817918937684224e-08
16	0.0024462	7.162168504567594e-10	-5.214470170820809e-10
17	0.0028244	-5.3479898470696436e-05	-5.978290548513011e-08
18	0.0030722	1.0324467392140866e-08	-3.343548861846317e-10
19	0.0031405	-2.586757937840435e-09	7.681985704178315e-10
20	0.0034162	1.987942481847199e-05	1.2839330971050634e-08
21	0.0036092	1.1203087677586033e-08	-1.9141011180586045e-10
22	0.0037397	-3.745565400809295e-09	-7.502872194244681e-10
23	0.0039021	-5.839707973218567e-05	-6.9937819402209e-08
24	0.0043558	-1.198532484532647e-08	-1.5298448783847332e-11
25	0.0044143	-5.815111948848173e-05	-2.853075011510423e-08
26	0.0044535	-2.2187235430718945e-09	-5.934036076937854e-10
27	0.0045541	4.75013635772344e-10	-1.0294695213324677e-09
28	0.004712	0.00013579844341405392	1.0875270378652661e-07
29	0.0048109	1.1226715079204604e-07	-1.0345834803003575e-06
30	0.0048773	-8.07882154051691e-09	4.782553405222497e-11
31	0.0049855	6.524115354941657e-07	-1.3596290574005839e-05
32	0.0050807	-9.1180134119489e-05	-9.13654595953416e-08
33	0.0052753	-1.0381186061475347e-06	1.1699443439323087e-05
34	0.0053127	-6.895521957644918e-08	4.0983616827455336e-09
35	0.0053129	2.6033264755044456e-05	6.184540396281813e-08
36	0.0053464	-4.205590179405217e-09	3.390678022139171e-10
37	0.0053726	-4.407556646962396e-09	1.73452438790857e-09
38	0.005548	1.8280083617620572e-09	1.657586915599903e-09
39	0.0057395	7.012222436339245e-08	-2.232783626052466e-10
40	0.0057591	2.9476702193041202e-08	-7.859796215780025e-10
41	0.005836	-1.3813511911400375e-07	5.799352633790776e-06
42	0.0059218	-1.5083603112260013e-05	-4.241200458798523e-08
43	0.0059608	0.00036270708856476455	4.384386671792897e-07
44	0.0060464	-3.926731582327267e-09	-6.6706770877266725e-12
45	0.0060585	3.965685053198059e-08	-1.7620596721093187e-10
46	0.0062956	6.840078647396124e-08	-2.037733592659845e-05
47	0.0064666	1.1155192756624154e-09	-4.194696653429829e-09
48	0.0065128	-0.0003823334193712708	-4.364117764129561e-07
49	0.0067295	-2.1789746166942837e-06	-1.4779160716197656e-05
50	0.0067562	0.0006897321923651079	7.012560865614287e-07
51	0.0069176	2.928240501776177e-09	1.643647251856188e-09
52	0.0069796	-9.136371881888345e-09	1.0870745329840085e-10
53	0.0070121	-2.4578023373599638e-09	-1.3263306606740645e-09
54	0.0071426	3.2694203832613814e-09	9.164687769442013e-11
55	0.0073223	-2.627782605750769e-06	2.205064637975563e-05
56	0.007339	2.0926113486577002e-08	7.083455576360665e-10
57	0.007342	-6.320760164872418e-06	-2.710145773242096e-07
58	0.0073924	-9.544536252078463e-11	1.2185813197073063e-08
59	0.0075859	1.335459409291462e-06	-5.8138166718590205e-05
60	0.0074797	-1.8366874423998495e-07	-2.2384979550612285e-09
61	0.0074872	0.00042030406043134063	5.474838084492071e-07
62	0.0075688	9.389785941709214e-08	-2.957699922730364e-10
63	0.0075837	-0.0008227476805976259	-8.788561864359834e-07
64	0.0078091	6.906487967963711e-10	1.7398110819943642e-10
65	0.0078638	0.0003016739244355037	3.3749986449016244e-07
66	0.0079243	0.0005635585565422213	6.344618215775848e-07
67	0.0082062	-4.524421589966501e-07	2.7774304925092188e-06

68	0.0082415	-1.250441014544069e-09	2.4565800677771527e-10
69	0.0082545	4.431235746282351e-09	-1.3910698647064783e-10
70	0.0082611	1.0536946512884557e-08	-1.0310628934888503e-09
71	0.0082762	2.134241185039779e-05	9.60863401380654e-08
72	0.0082851	3.662018213119973e-05	1.403294263065983e-07
73	0.0083019	-1.1352899444811443e-07	4.8702663011561906e-06
74	0.0083351	-1.4224036584739226e-07	1.999399237521111e-10
75	0.0087153	0.0010192583090057202	1.0902086950511816e-06
76	0.016243	-1.99813019275822e-07	-4.094905159670978e-09
77	0.016246	0.00012529425562245302	1.658124506762384e-07
78	0.016513	-2.542044728916468e-06	-2.8974838008092468e-05
79	0.016494	-5.0613856562605464e-08	6.308045655380595e-08
80	0.016497	-9.603764115181505e-08	-7.381740908732032e-08
81	0.016499	1.0189685759936809e-05	-3.559691430184785e-06
82	0.016635	-6.936756119795116e-05	-1.131654832766754e-07
83	0.016791	8.979770730602814e-08	1.1862020696126103e-10
84	0.016795	-3.123770525297914e-05	-5.418518479639523e-09
85	0.016812	2.6711482533195344e-08	-6.326942875053638e-09
86	0.016824	-2.3475735617918343e-05	2.9115411758407263e-08
87	0.017022	-2.8181171586717257e-07	2.2611476146731332e-06
88	0.017028	-2.358892658645577e-08	-1.885861409677816e-09
89	0.01703	1.5089604242888545e-08	-3.6248718935805167e-09
90	0.017035	-2.7235232369331824e-06	-1.342901738860666e-07
91	0.017042	1.4297289647929777e-06	-8.195615815349083e-06
92	0.017041	4.782115092430232e-09	-3.5881854487928854e-07
93	0.017132	-1.861114475751559e-08	5.932948657209837e-09
94	0.017152	-6.348297678575571e-05	-5.7493917869632086e-08
95	0.017487	-9.247300545130292e-09	1.2934768915920066e-12

C. Retinal model

The retinal model parameters are given below

$$
\begin{aligned}
\Omega_c &= 1532\text{cm}^{-1} = 0.006980305650817135 \quad \text{a.u. in energy,} \\
E_1 &= 2.48\ \text{eV} = 0.0911383298673206 \quad \text{a.u. in energy,} \\
W_0 &= 3.6\ \text{eV} = 0.13229757561385247 \quad \text{a.u. in energy,} \\
W_1 &= 1.09\ \text{eV} = 0.04005676594974978 \quad \text{a.u. in energy,} \\
\kappa &= 0.1\ \text{eV} = 0.003674932655940347 \quad \text{a.u. in energy,} \\
\lambda &= 0.19\ \text{eV} = 0.006982372046286658 \quad \text{a.u. in energy,}
\end{aligned}
\tag{S8}
$$

$$\omega_j = \begin{cases} 792.8\text{cm}^{-1} = 0.003612262599753153 & \text{a.u. in energy} \\ 842.8\text{cm}^{-1} = 0.003840079363107918 & \text{a.u. in energy} \\ 866.2\text{cm}^{-1} = 0.003946697608357949 & \text{a.u. in energy} \\ 882.4\text{cm}^{-1} = 0.004020510239684892 & \text{a.u. in energy} \\ 970.3\text{cm}^{-1} = 0.004421012109662569 & \text{a.u. in energy} \\ 976.0\text{cm}^{-1} = 0.004446983220685013 & \text{a.u. in energy} \\ 997.0\text{cm}^{-1} = 0.004542666261294013 & \text{a.u. in energy} \\ 1017.1\text{cm}^{-1} = 0.004634248600162629 & \text{a.u. in energy} \\ 1089.6\text{cm}^{-1} = 0.004964582907027038 & \text{a.u. in energy} \\ 1189.0\text{cm}^{-1} = 0.005417482632576311 & \text{a.u. in energy} \\ 1214.7\text{cm}^{-1} = 0.005534580448940661 & \text{a.u. in energy} \\ 1238.1\text{cm}^{-1} = 0.005641198694190689 & \text{a.u. in energy} \\ 1267.9\text{cm}^{-1} = 0.00577697748515013 & \text{a.u. in energy} \\ 1317.0\text{cm}^{-1} = 0.006000693546764509 & \text{a.u. in energy} \\ 1359.0\text{cm}^{-1} = 0.006192059627982512 & \text{a.u. in energy} \\ 1389.0\text{cm}^{-1} = 0.006328749685995371 & \text{a.u. in energy} \\ 1428.4\text{cm}^{-1} = 0.006508269295518926 & \text{a.u. in energy} \\ 1434.9\text{cm}^{-1} = 0.006537885474755045 & \text{a.u. in energy} \\ 1451.8\text{cm}^{-1} = 0.006614887540768955 5 & \text{a.u. in energy} \\ 1572.8\text{cm}^{-1} = 0.007166204108087487 & \text{a.u. in energy} \\ 1612.1\text{cm}^{-1} = 0.007345268084084332 & \text{a.u. in energy} \\ 1629.2\text{cm}^{-1} = 0.007423181417151662 & \text{a.u. in energy} \\ 1659.1\text{cm}^{-1} = 0.007559415841637810 5 & \text{a.u. in energy} \end{cases}$$

$$c_j = \begin{cases} 0.175, 0.2, 0.175, 0.225, 0.55, \\ 0.3, 0.33, 0.45, 0.125, 0.175, \\ 0.44, 0.5, 0.475, 0.238, 0.25 \\ 0.25, 0.25, 0.225, 0.225, 0.25 \\ 0.225, 0.125, 0.225 \end{cases}$$

II. SUPPLEMENTAL FIGURES AND TABLES

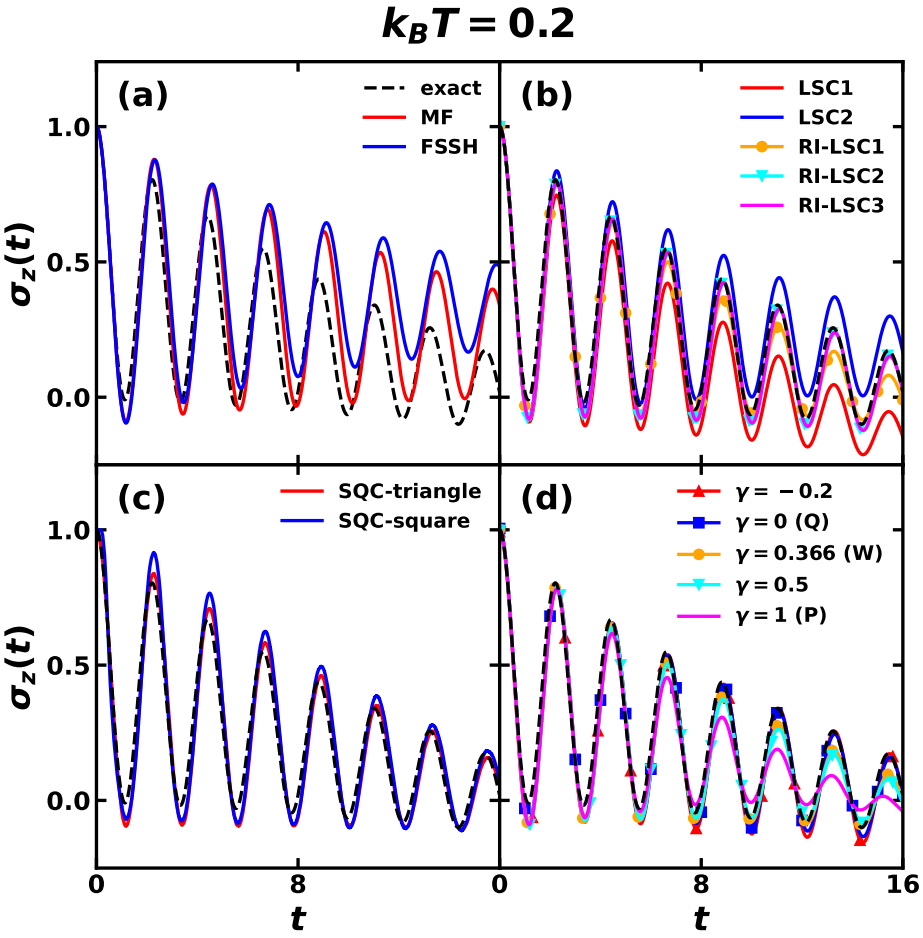

FIG. S1. Population difference dynamics of spin-boson model #1 at $k_BT = 0.2$ obtained with various approximate mixed quantum-classical, semiclassical, and quasiclassical dynamics methods (solid lines) in comparison with numerically exact dynamics at finite-temperature by TT-TFD (dashed line).

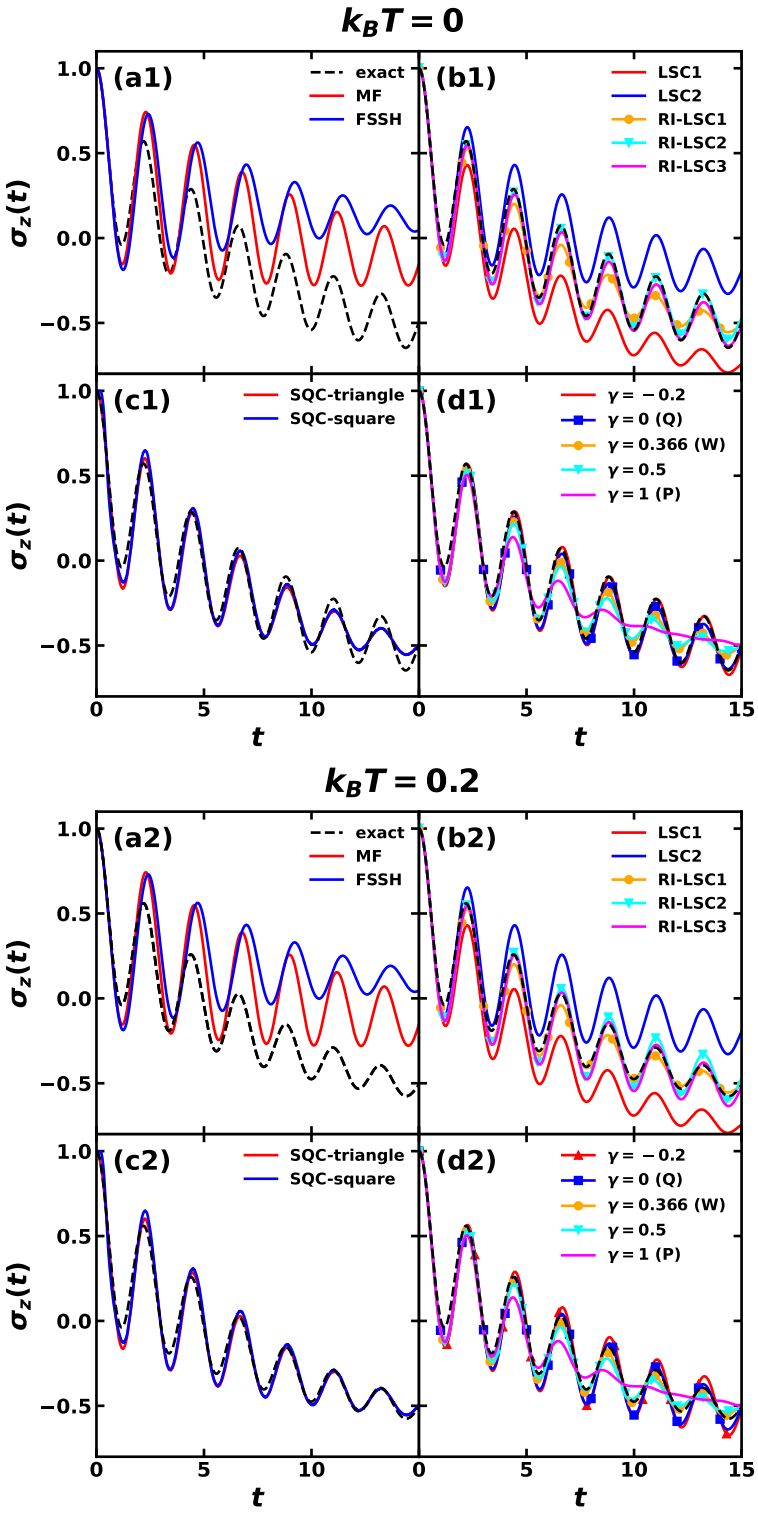

FIG. S2. Population difference dynamics of spin-boson model #2 at zero temperature (upper panels) and at $k_BT = 0.2$ (lower panels) obtained with various approximate mixed quantum-classical, semiclassical, and quasiclassical dynamics methods (solid lines) in comparison with numerically exact dynamics at zero temperature by TT-KSL and at finite-temperature by TT-TFD (dashed line).

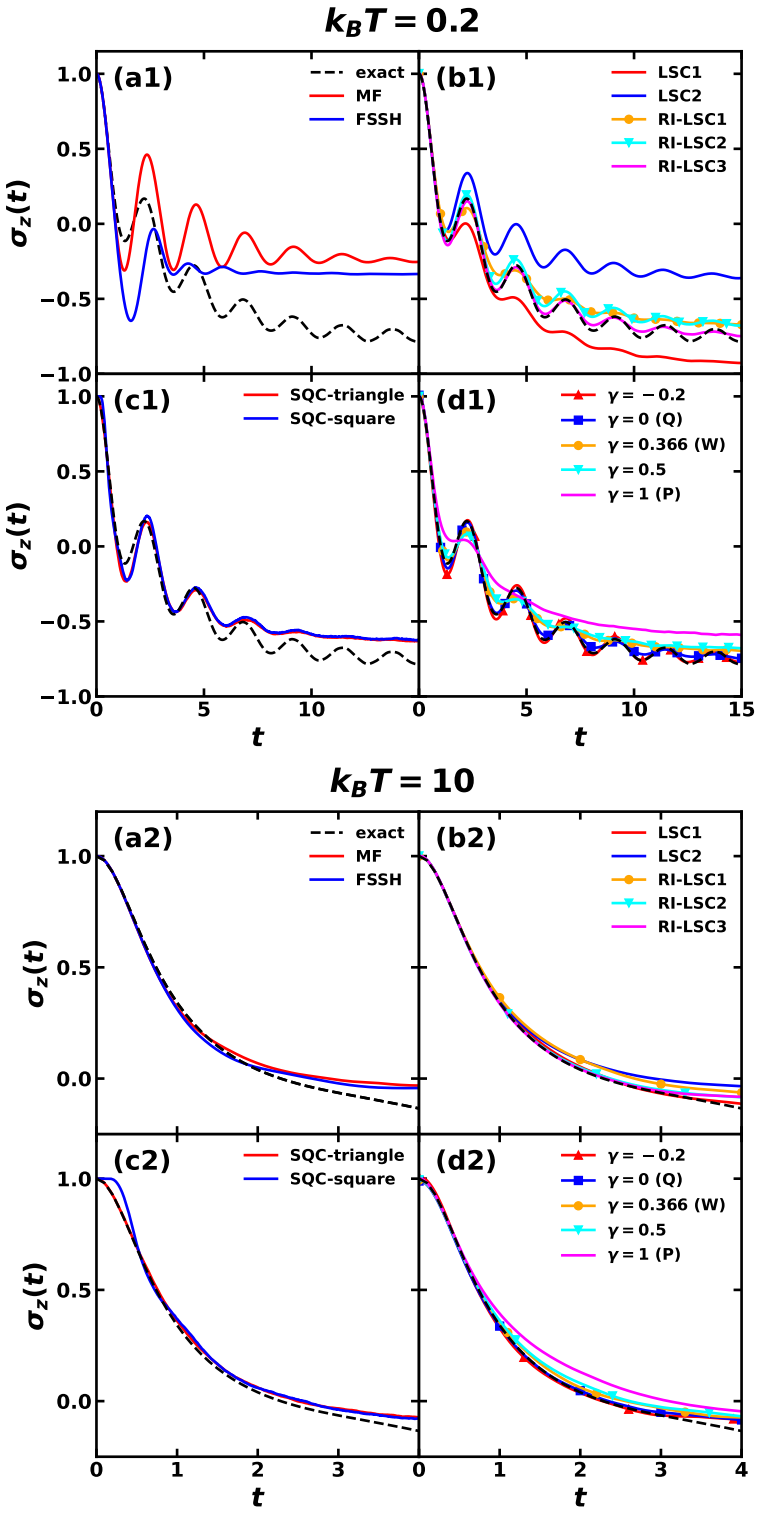

FIG. S3. Population difference dynamics of spin-boson model #3 at $k_BT = 0.2$ (upper panels) and at $k_BT = 10$ (lower panels) obtained with various approximate mixed quantum-classical, semiclassical, and quasiclassical dynamics methods (solid lines) in comparison with numerically exact dynamics at finite-temperature by TT-TFD (dashed line).

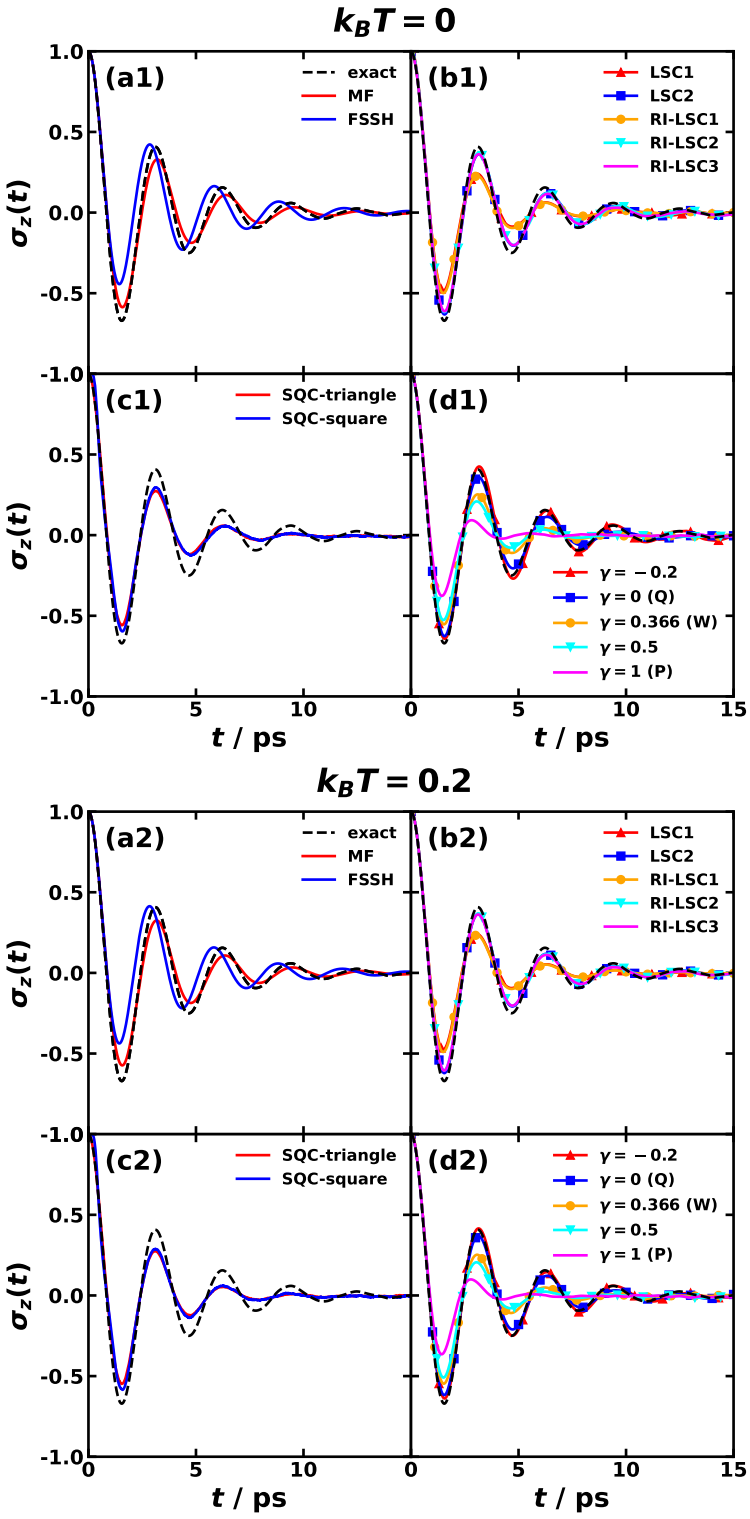

FIG. S4. Population difference dynamics of spin-boson model #4 at zero temperature (upper panels) and at $k_BT = 0.2$ (lower panels) obtained with various approximate mixed quantum-classical, semiclassical, and quasiclassical dynamics methods (solid lines) in comparison with numerically exact dynamics at zero temperature by TT-KSL and at finite-temperature by TT-TFD (dashed line).

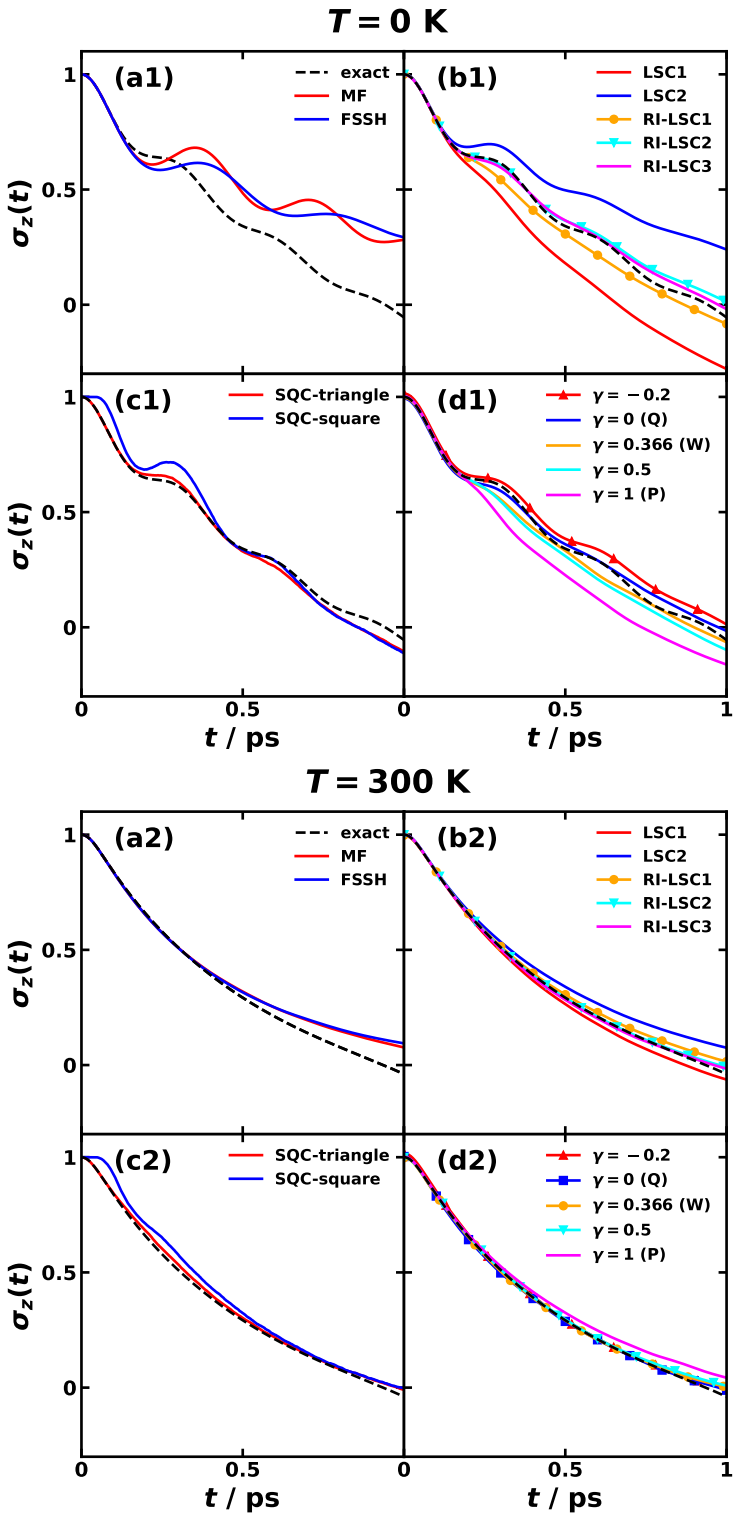

FIG. S5. Population difference dynamics of spin-boson model #5 at zero temperature (upper panels) and at $k_B T = 0.2$ (lower panels) obtained with various approximate mixed quantum-classical, semiclassical, and quasiclassical dynamics methods (solid lines) in comparison with numerically exact dynamics at zero temperature by TT-KSL and at finite-temperature by TT-TFD (dashed line).

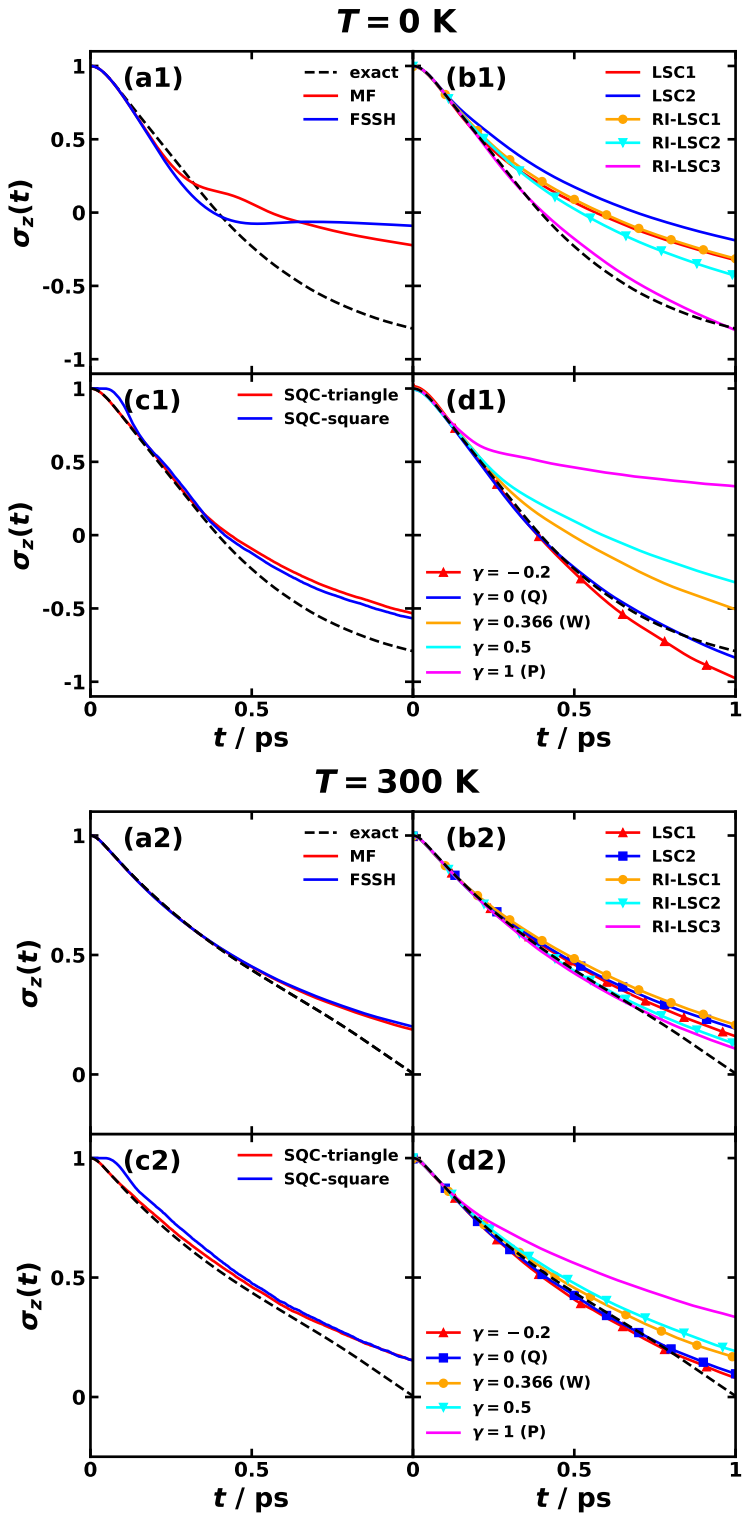

FIG. S6. Population difference dynamics of spin-boson model #6 at zero temperature (upper panels) and at $k_B T = 0.2$ (lower panels) obtained with various approximate mixed quantum-classical, semiclassical, and quasiclassical dynamics methods (solid lines) in comparison with numerically exact dynamics at zero temperature by TT-KSL and at finite-temperature by TT-TFD (dashed line).

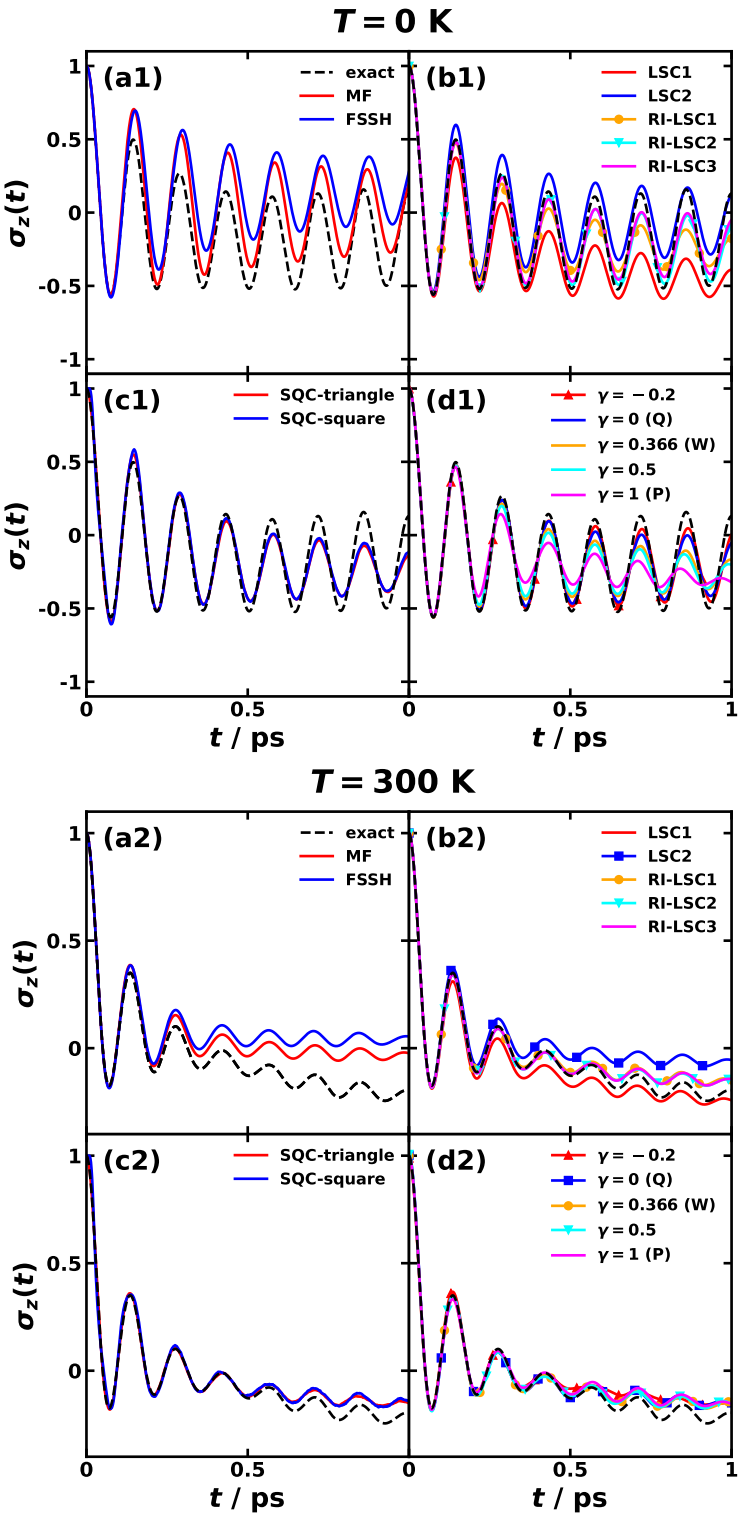

FIG. S7. Population difference dynamics of spin-boson model #7 at zero temperature (upper panels) and at $k_B T = 0.2$ (lower panels) obtained with various approximate mixed quantum-classical, semiclassical, and quasiclassical dynamics methods (solid lines) in comparison with numerically exact dynamics at zero temperature by TT-KSL and at finite-temperature by TT-TFD (dashed line).

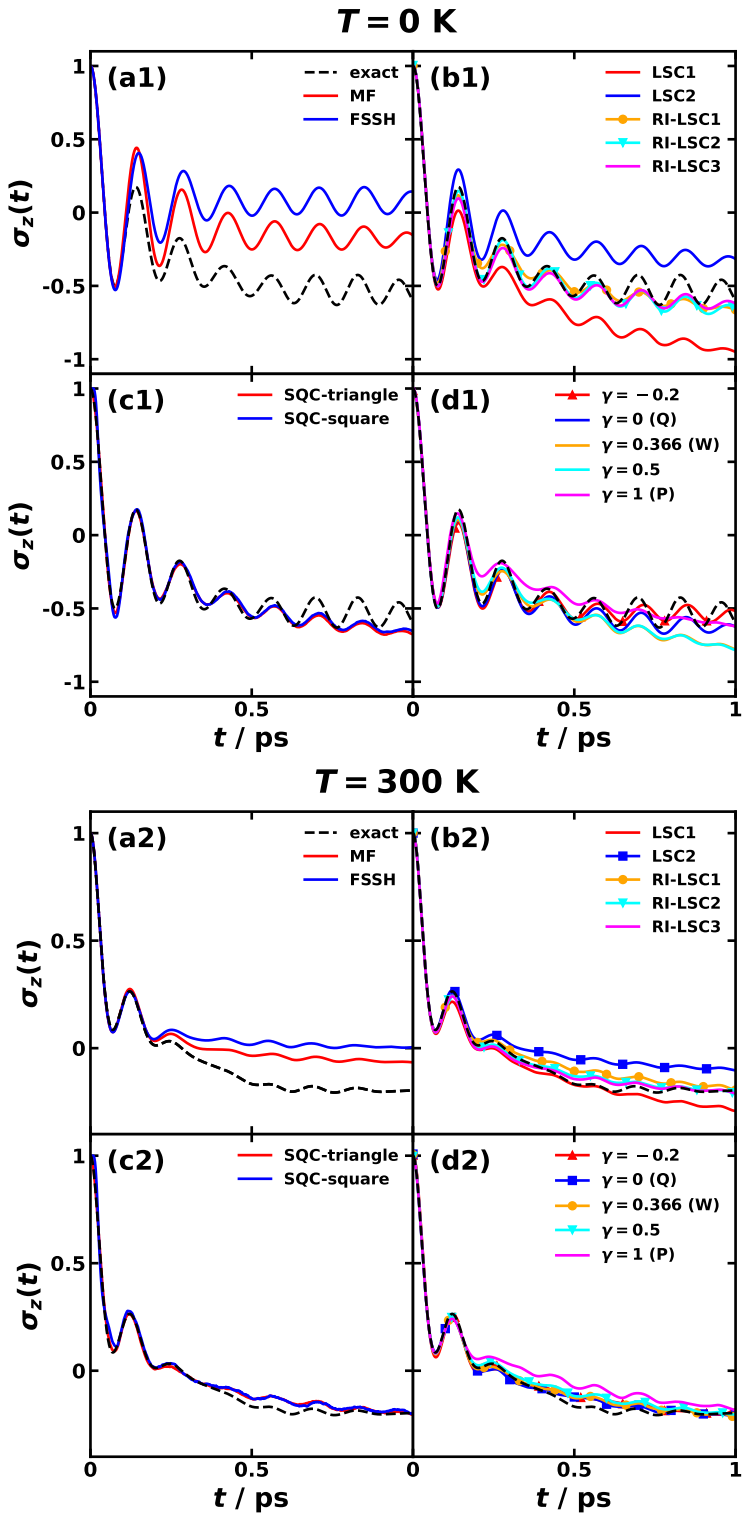

FIG. S8. Population difference dynamics of spin-boson model #8 at zero temperature (upper panels) and at $k_B T = 0.2$ (lower panels) obtained with various approximate mixed quantum-classical, semiclassical, and quasiclassical dynamics methods (solid lines) in comparison with numerically exact dynamics at zero temperature by TT-KSL and at finite-temperature by TT-TFD (dashed line).

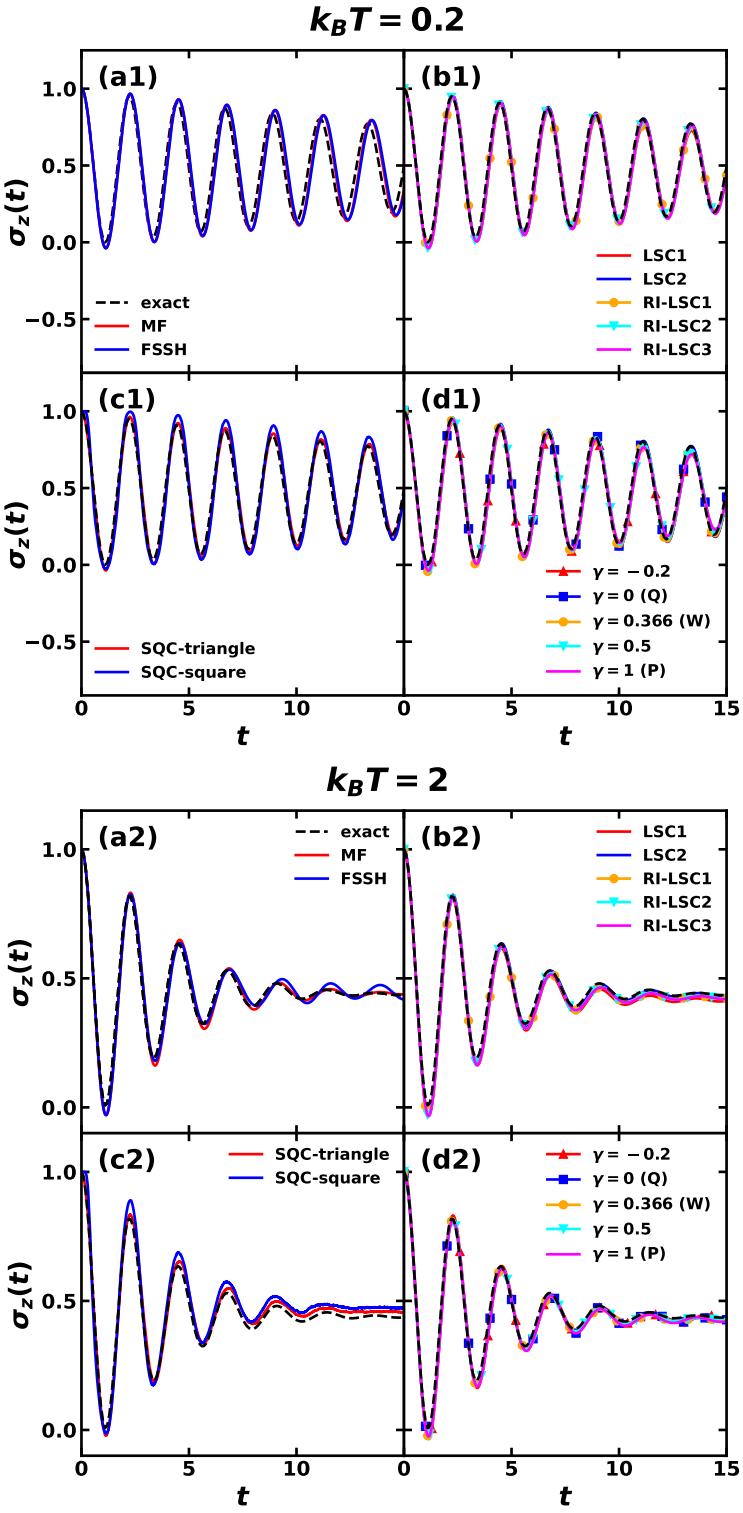

FIG. S9. Population difference dynamics of spin-boson model #9 at $k_BT = 0.2$ (upper panels) and $k_BT = 2$ (lower panels) obtained with various approximate mixed quantum-classical, semiclassical, and quasiclassical dynamics methods (solid lines) in comparison with numerically exact dynamics at finite-temperature by TT-TFD (dashed line).

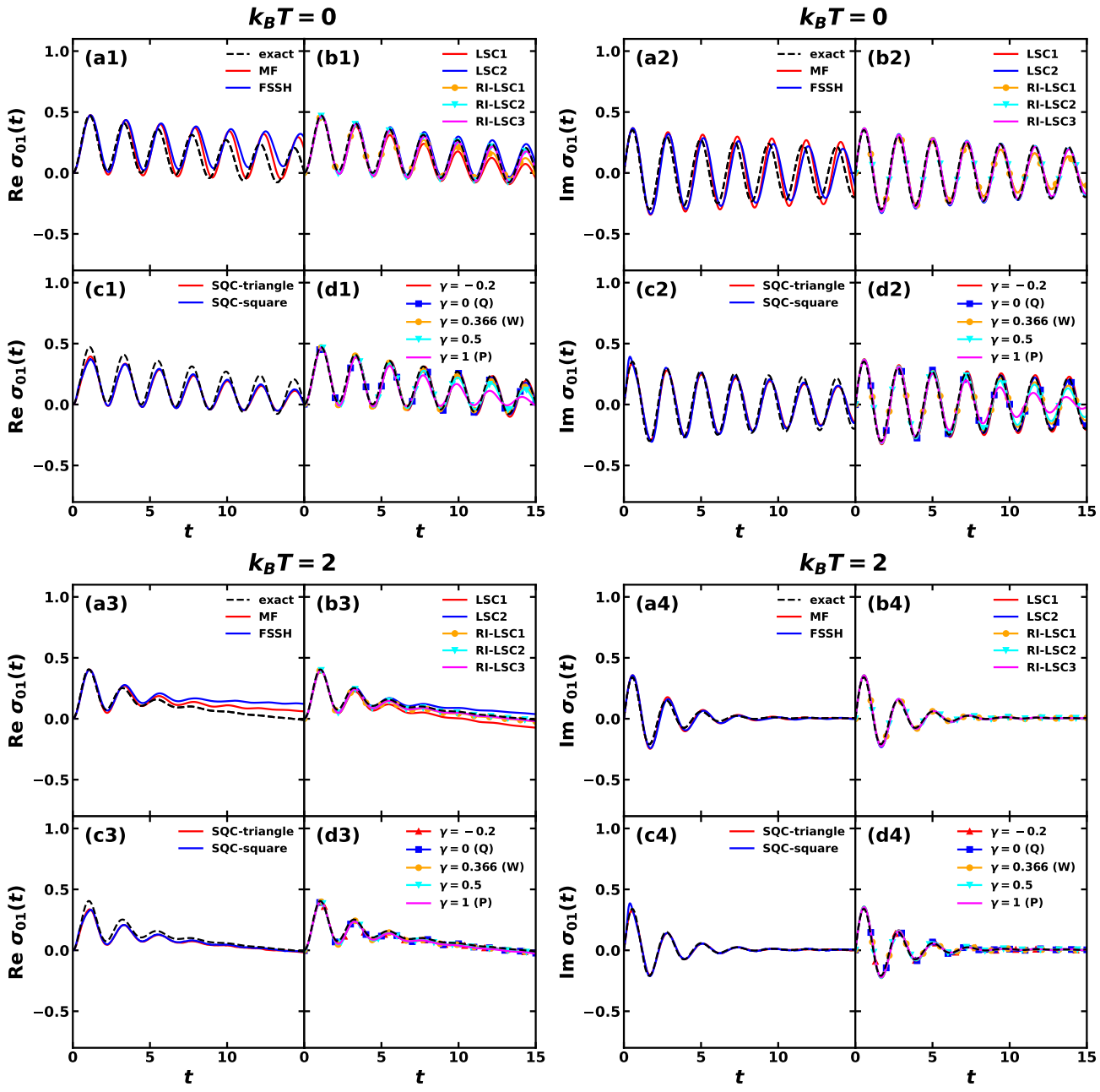

FIG. S10. Coherence dynamics of spin-boson model #1 at zero temperature (upper panels) and at $k_BT = 0.2$ (lower panels) obtained with various approximate mixed quantum-classical, semiclassical, and quasiclassical dynamics methods (solid lines) in comparison with numerically exact dynamics at zero temperature by TT-KSL and at finite-temperature by TT-TFD (dashed line). The real and imaginary parts of $\sigma_{01}(t)$ are plotted in the left and right panels, respectively.

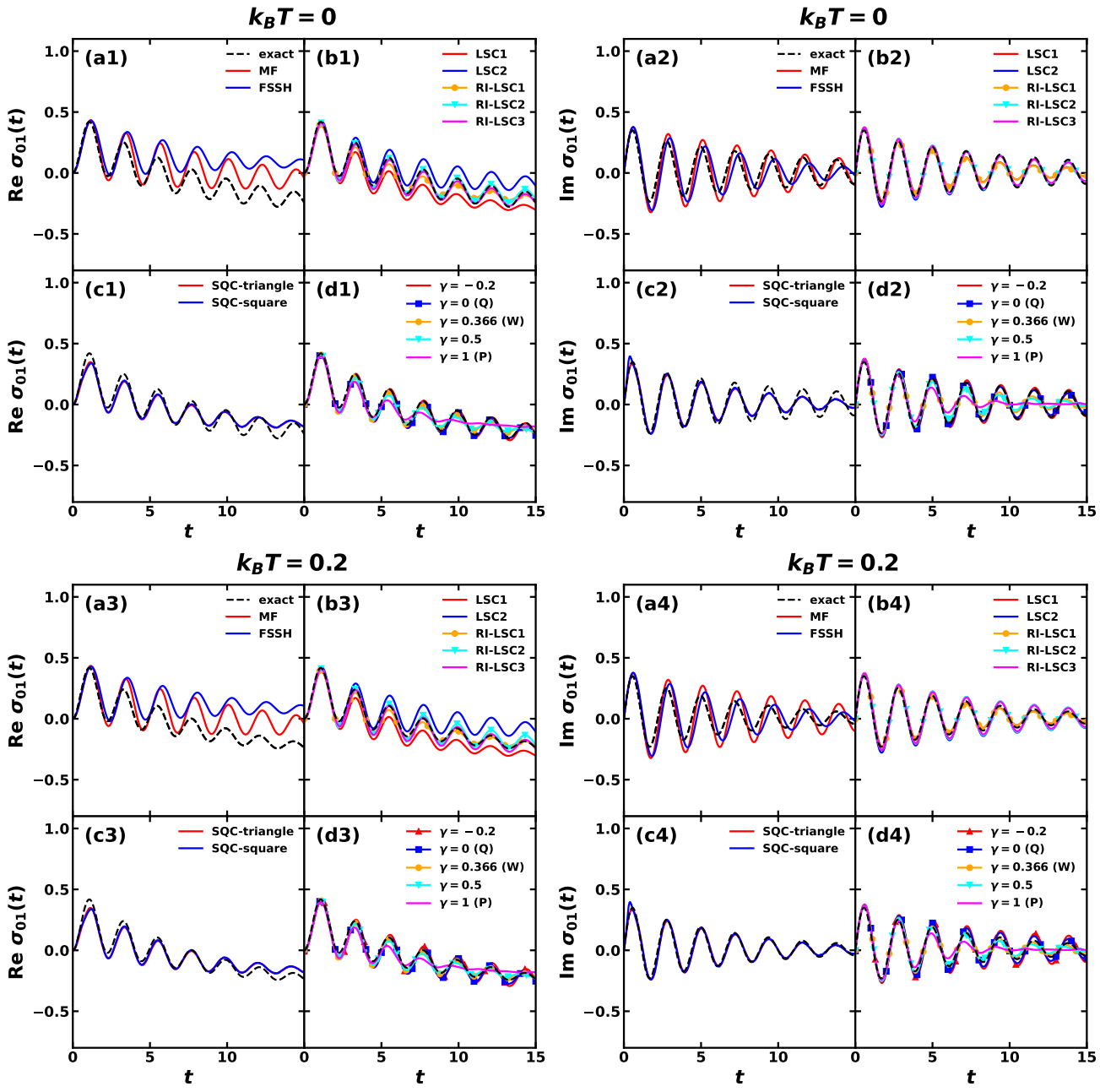

FIG. S11. Coherence dynamics of spin-boson model #2 at zero temperature (upper panels) and at $k_BT = 0.2$ (lower panels) obtained with various approximate mixed quantum-classical, semiclassical, and quasiclassical dynamics methods (solid lines) in comparison with numerically exact dynamics at zero temperature by TT-KSL and at finite-temperature by TT-TFD (dashed line). The real and imaginary parts of $\sigma_{01}(t)$ are plotted in the left and right panels, respectively.

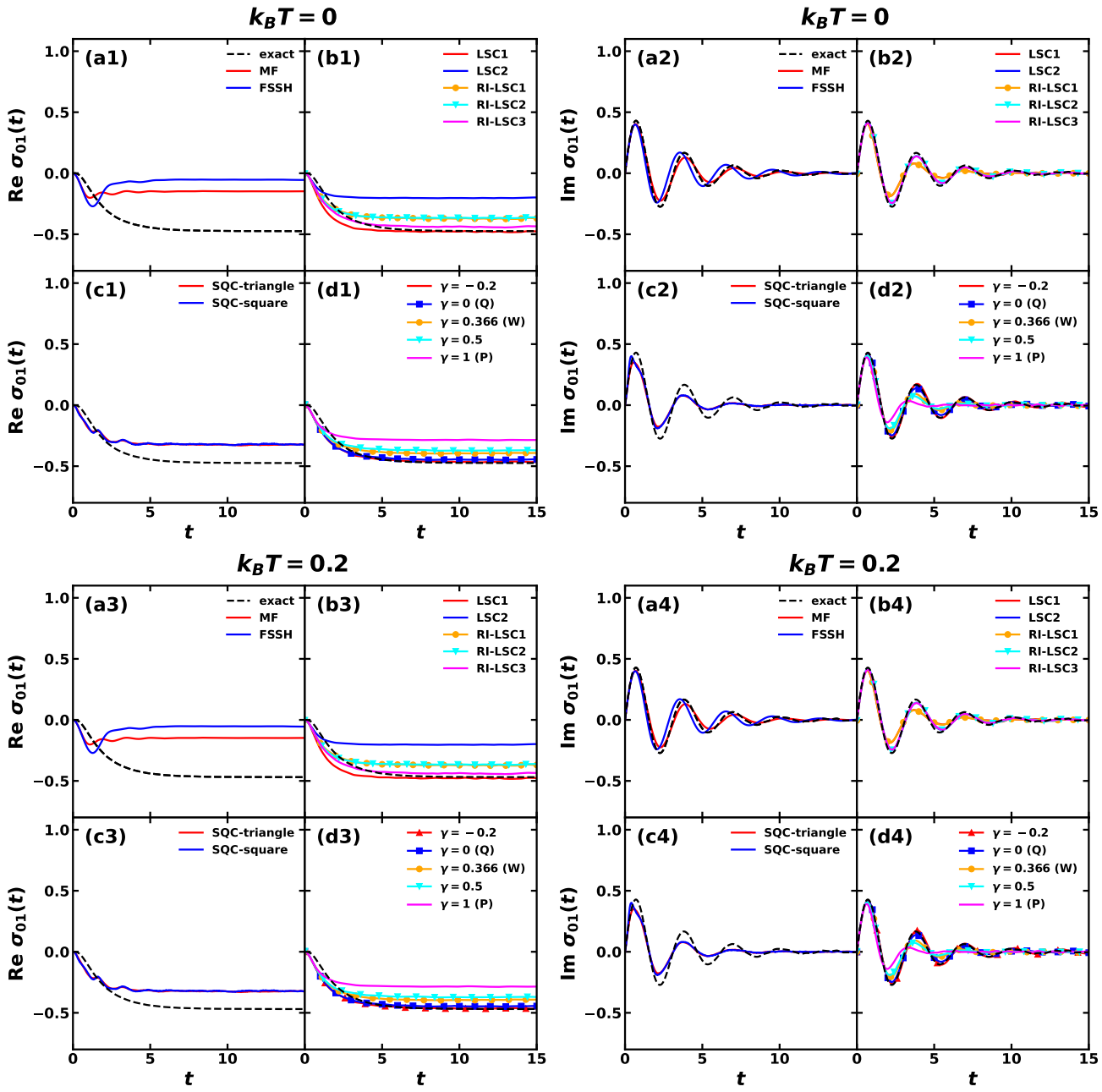

FIG. S12. Coherence dynamics of spin-boson model #4 at zero temperature (upper panels) and at $k_BT = 0.2$ (lower panels) obtained with various approximate mixed quantum-classical, semiclassical, and quasiclassical dynamics methods (solid lines) in comparison with numerically exact dynamics at zero temperature by TT-KSL and at finite-temperature by TT-TFD (dashed line). The real and imaginary parts of $\sigma_{01}(t)$ are plotted in the left and right panels, respectively.

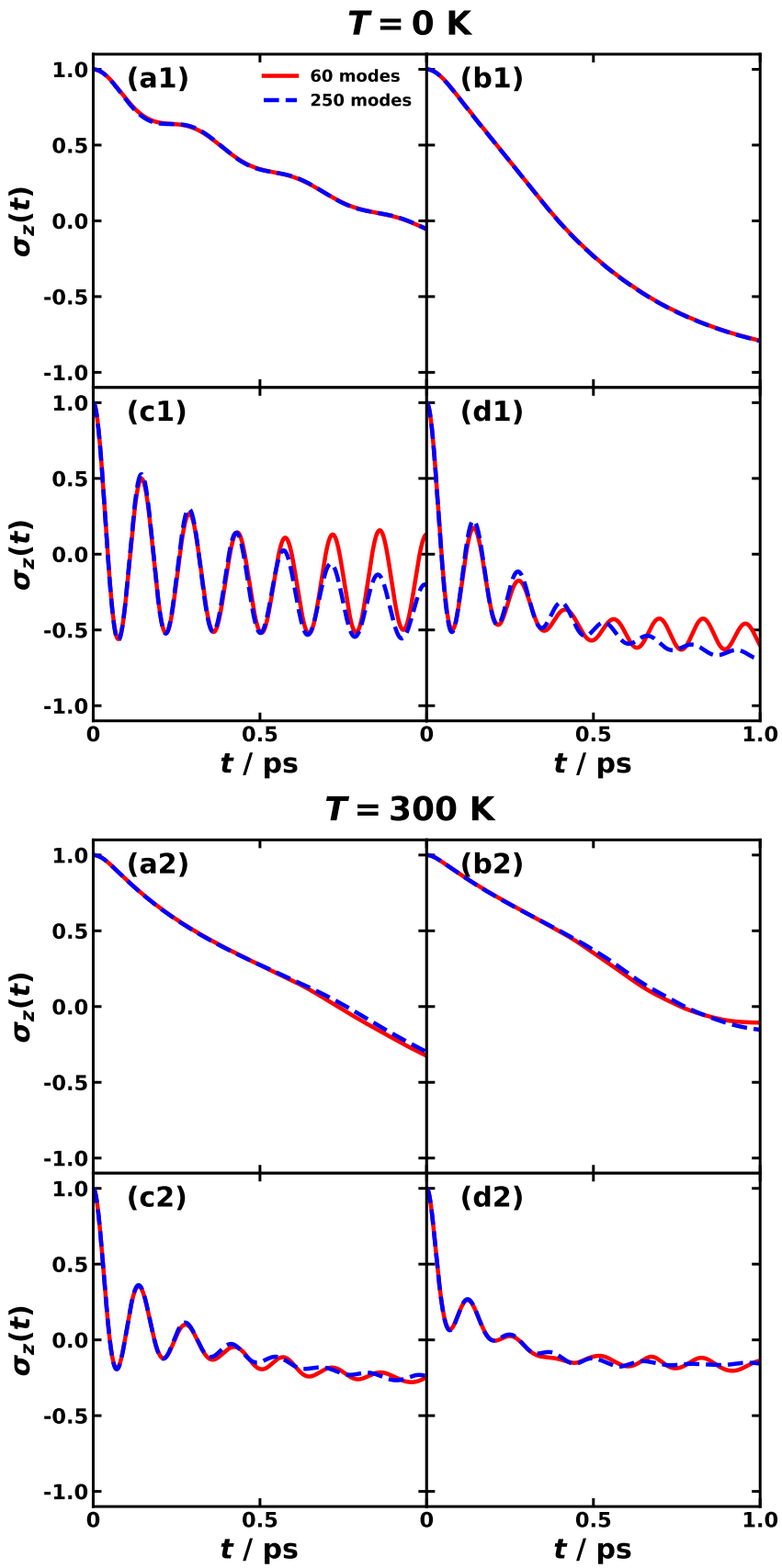

FIG. S13. Comparison of $N = 60$ (solid red) and $N = 250$ (dash blue) modes in spin-boson models #5–#8 (a,b,c,d) at zero temperature (upper panels) and 300 K (lower panels), and the numerically exact population dynamics is obtained with tensor-train methods.

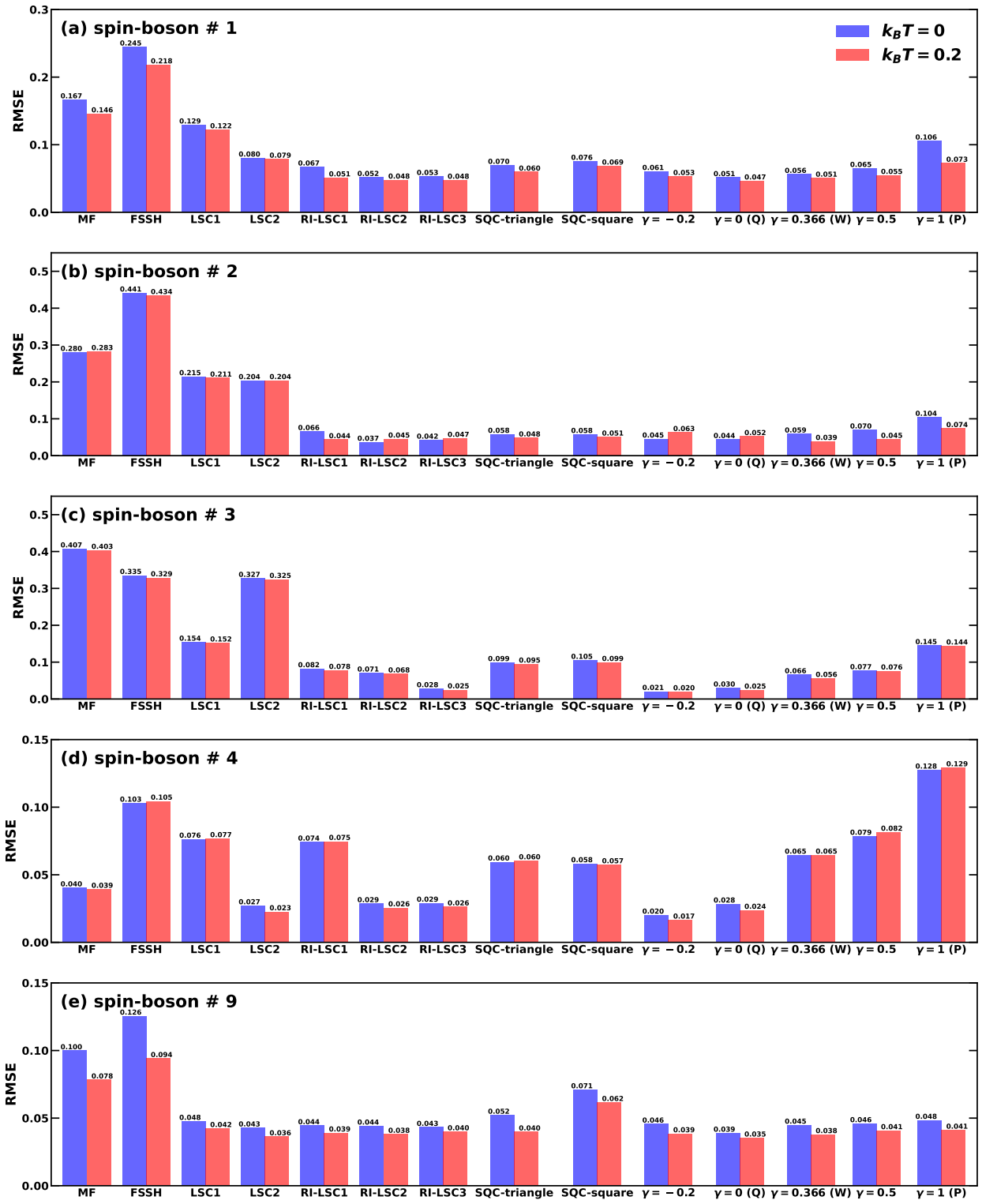

FIG. S14. Root-mean-square errors (RMSE) of the approximate methods for spin-boson models #1–#4 and #9 from the tensor-train method. The blue bars and red bars correspond to the RMSE for $k_BT = 0$ and $k_BT = 0.2$ cases, respectively.

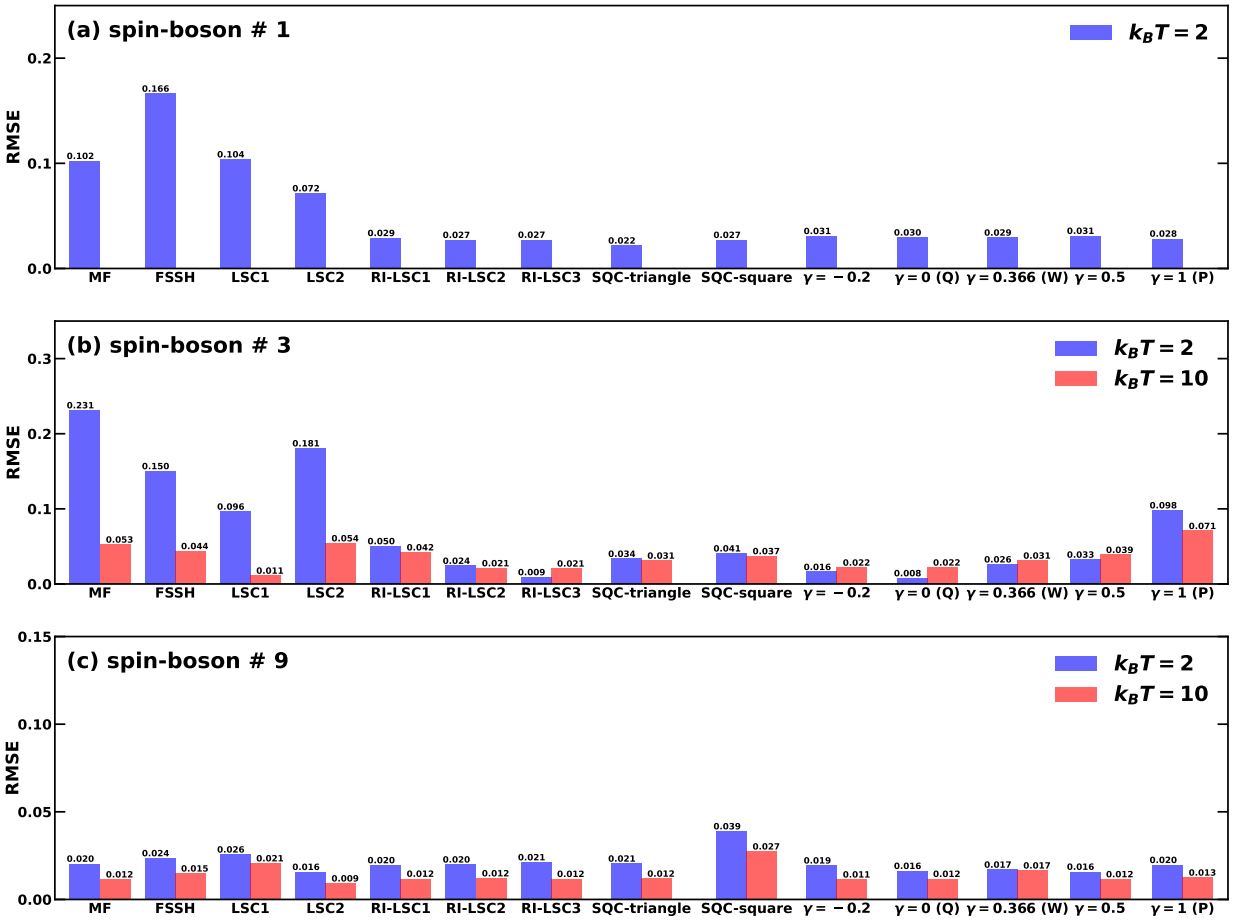

FIG. S15. Root-mean-square errors (RMSE) of the approximate methods for spin-boson models #1–#4 and #9 from the tensor-train method. The blue bars are zero-temperature RMSE and the red ones are finite-temperature RMSE. The blue bars and red bars correspond to the RMSE for $k_BT = 2$ and $k_BT = 10$ cases, respectively.

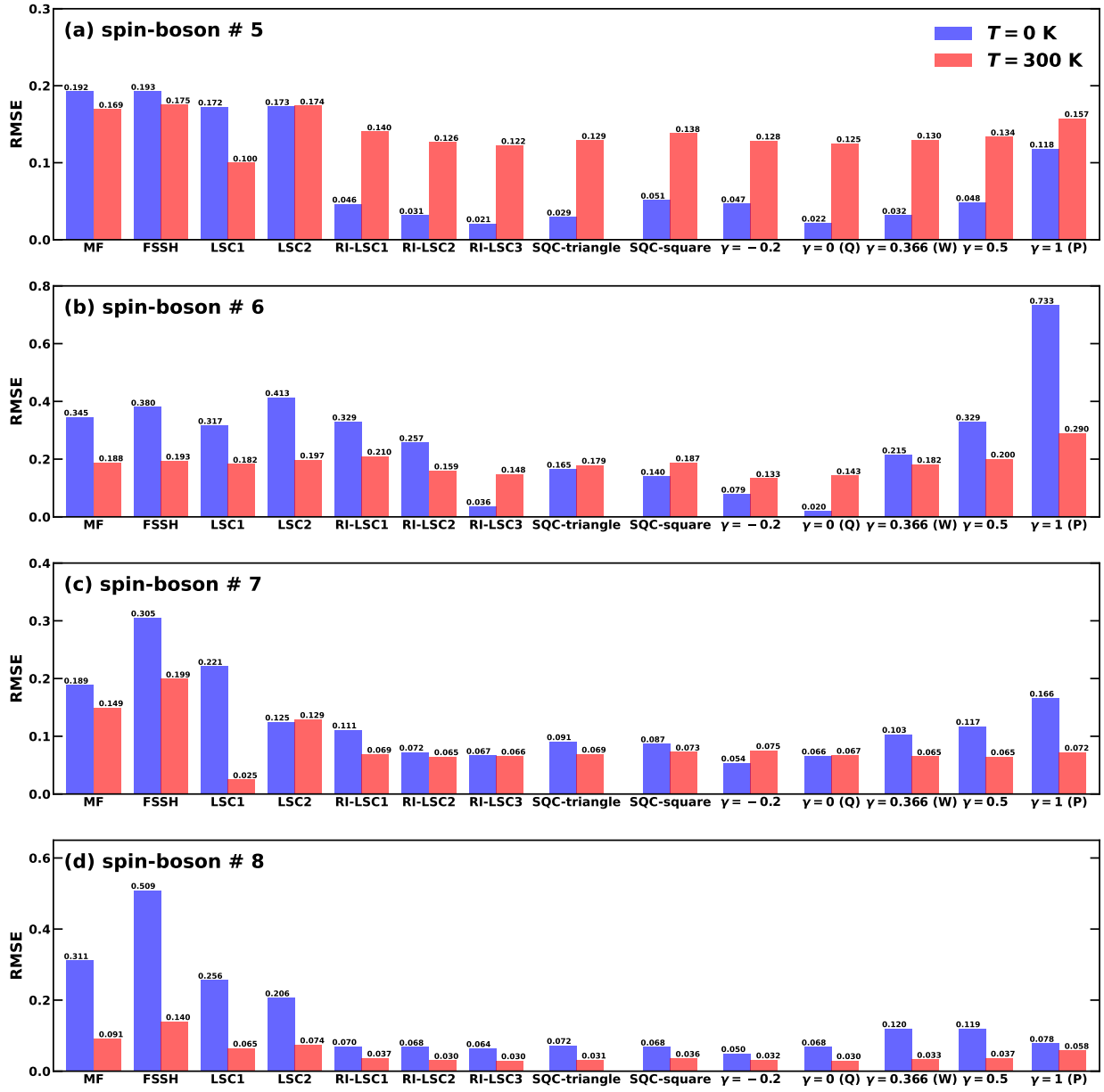

FIG. S16. Root-mean-square errors (RMSE) of the approximate methods for spin-boson models #5–#8 from the tensor-train method. The blue bars and red bars correspond to the RMSE for $T = 0$ and $T = 300$ K cases, respectively.

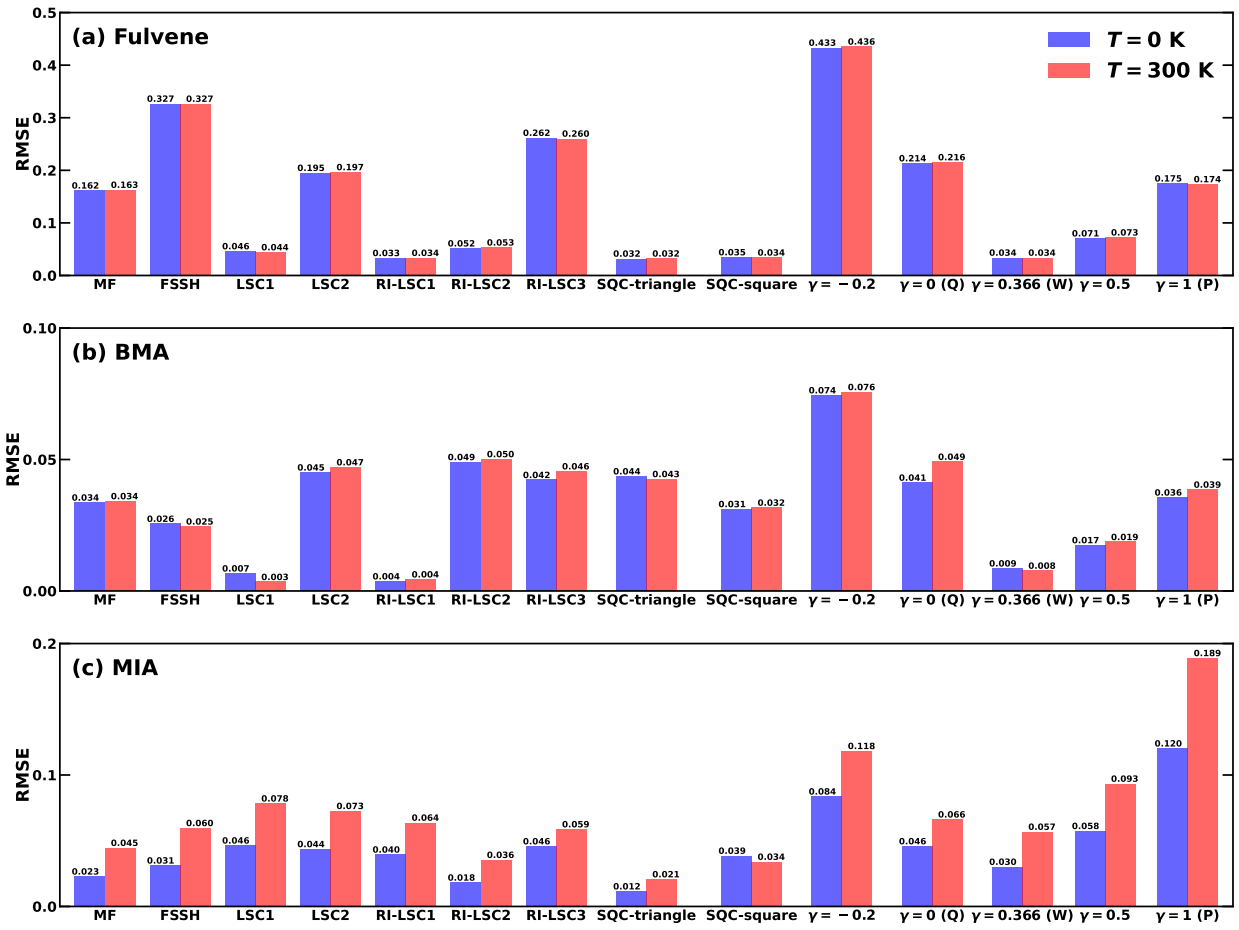

FIG. S17. Root-mean-square errors (RMSE) of the semiclassical methods for linear vibronic coupling models from the tensor-train method. The blue bars are zero-temperature RMSE and the red ones are finite-temperature RMSE.

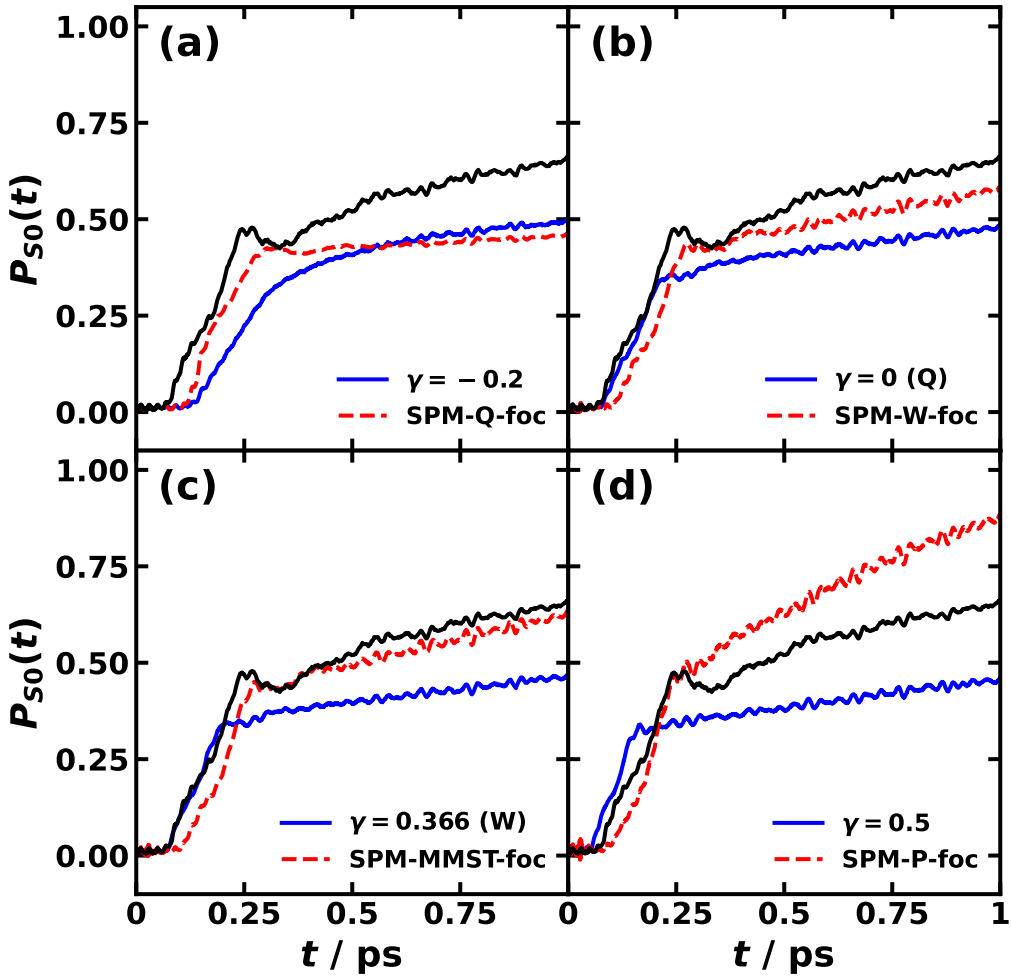

FIG. S18. Effects of focus initial sampling on the mapping variables in the retinal model at zero temperature. Plotted are the ground state (S_0) population as a function of time. Black lines are numerically exact results from TT-SOKSL, blue solid lines show the full sphere sampling of the spin mapping methods, and red dashed lines show the focused sampling of the spin mapping methods.

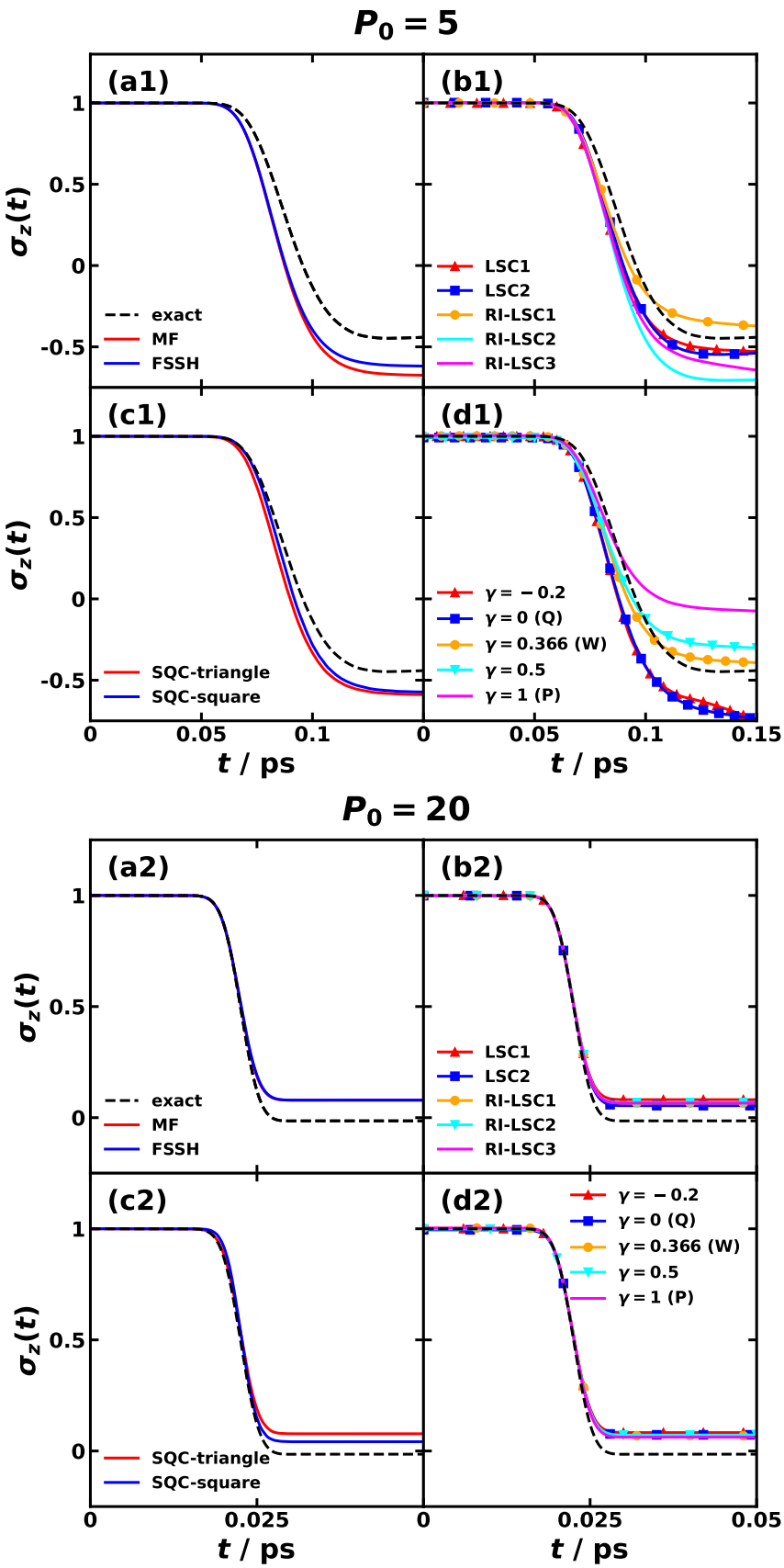

FIG. S19. Nonadiabatic dynamics of Tully's single avoid crossing (SAC) model at zero temperature with low initial momentum $p_0 = 5$ (upper panels) and high initial momentum $p_0 = 20$ (lower panels), where the exact result is obtained with SOFT method and the approximate results are obtained with various mixed quantum-classical, semiclassical, and quasiclassical dynamics methods.

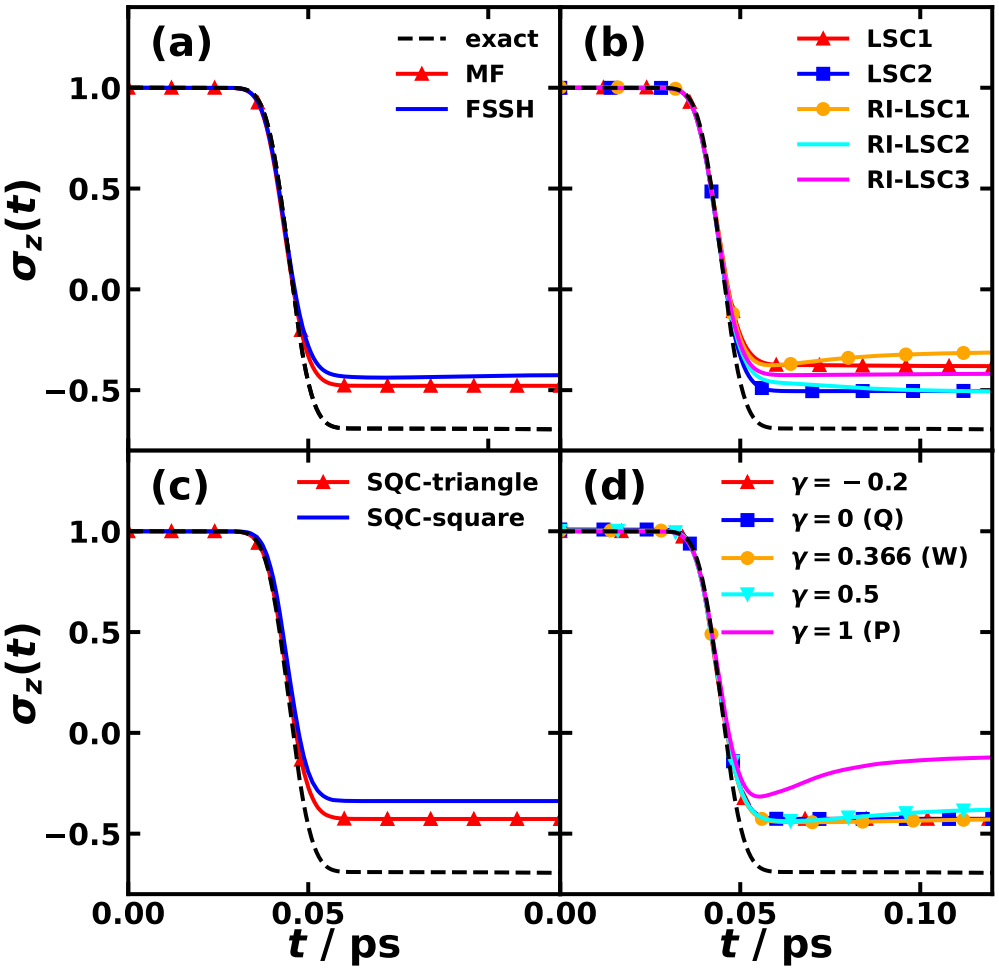

FIG. S20. Nonadiabatic dynamics of Tully's single avoid crossing (SAC) model at zero temperature with initial momentum $p_0 = 10$, where the exact result is obtained with SOFT method and the approximate results are obtained with various mixed quantum-classical, semiclassical, and quasiclassical dynamics methods.

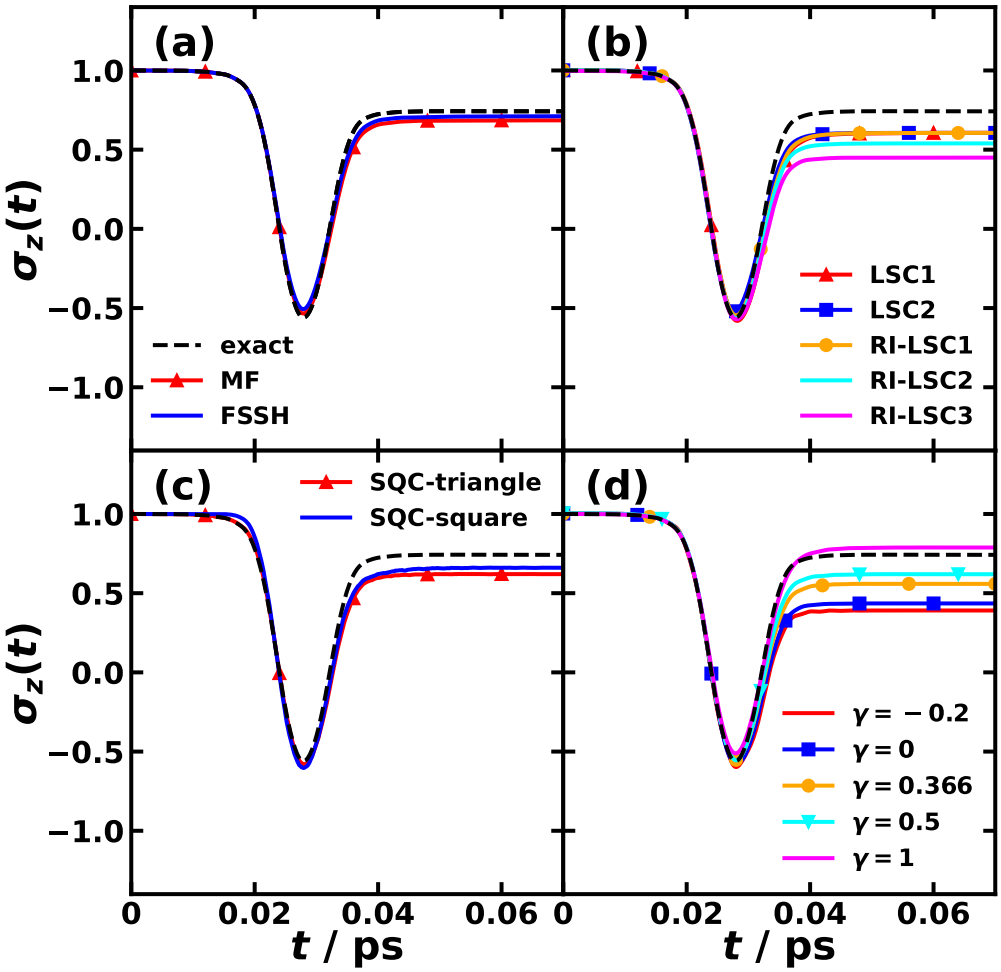

FIG. S21. Nonadiabatic dynamics of Tully's double avoid crossing (DAC) model at zero temperature with initial momentum $p_0 = 15$, where the exact result is obtained with SOFT method and the approximate results are obtained with various mixed quantum-classical, semiclassical, and quasiclassical dynamics methods.

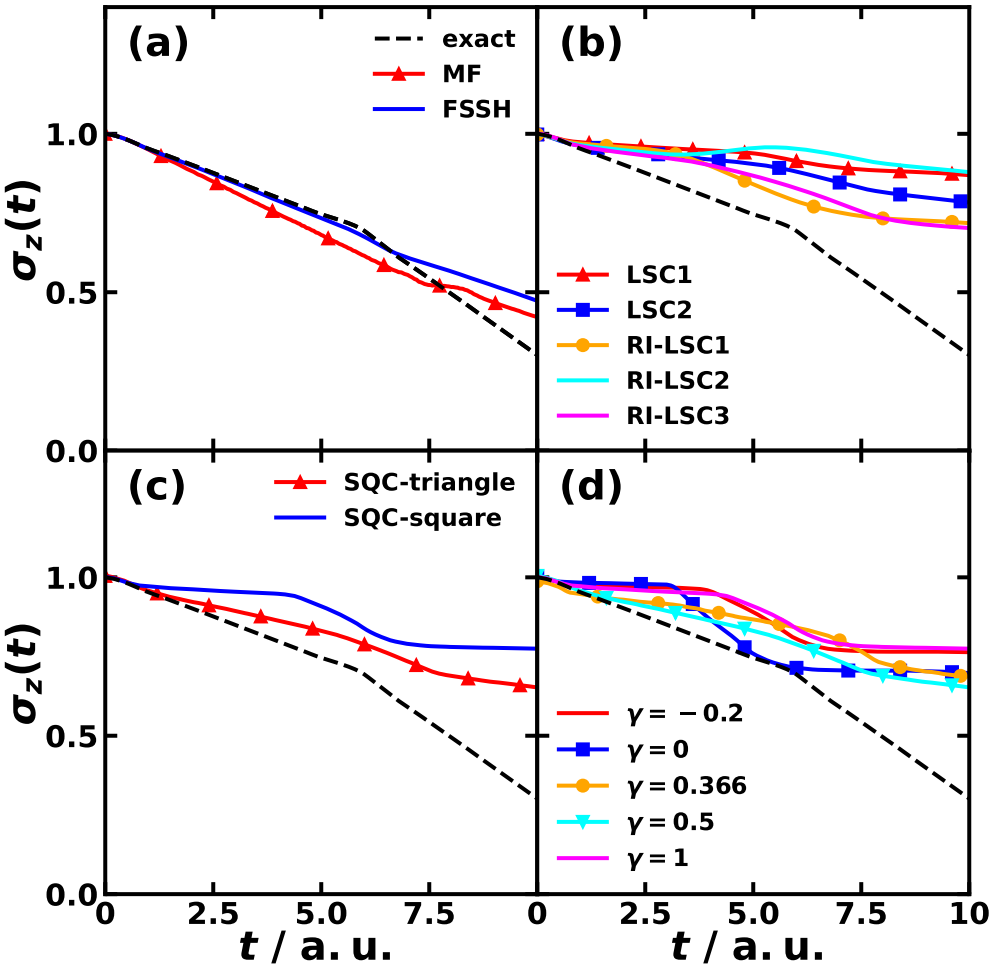

FIG. S22. Line cross parabola potentials are tested. In panel (a), mixed quantum-classical dynamics are benchmarked with the numerically exact results (black), in panel (b), LSC mapping dynamics are benchmarked, in panel (c), SQC dynamics are benchmarked, and in panel (d), SPM dynamics are benchmarked. The initial nuclear state is the vibrational eigenstate of $n = 15$ of the harmonic oscillator and electronic dynamics begins at the parabola state.

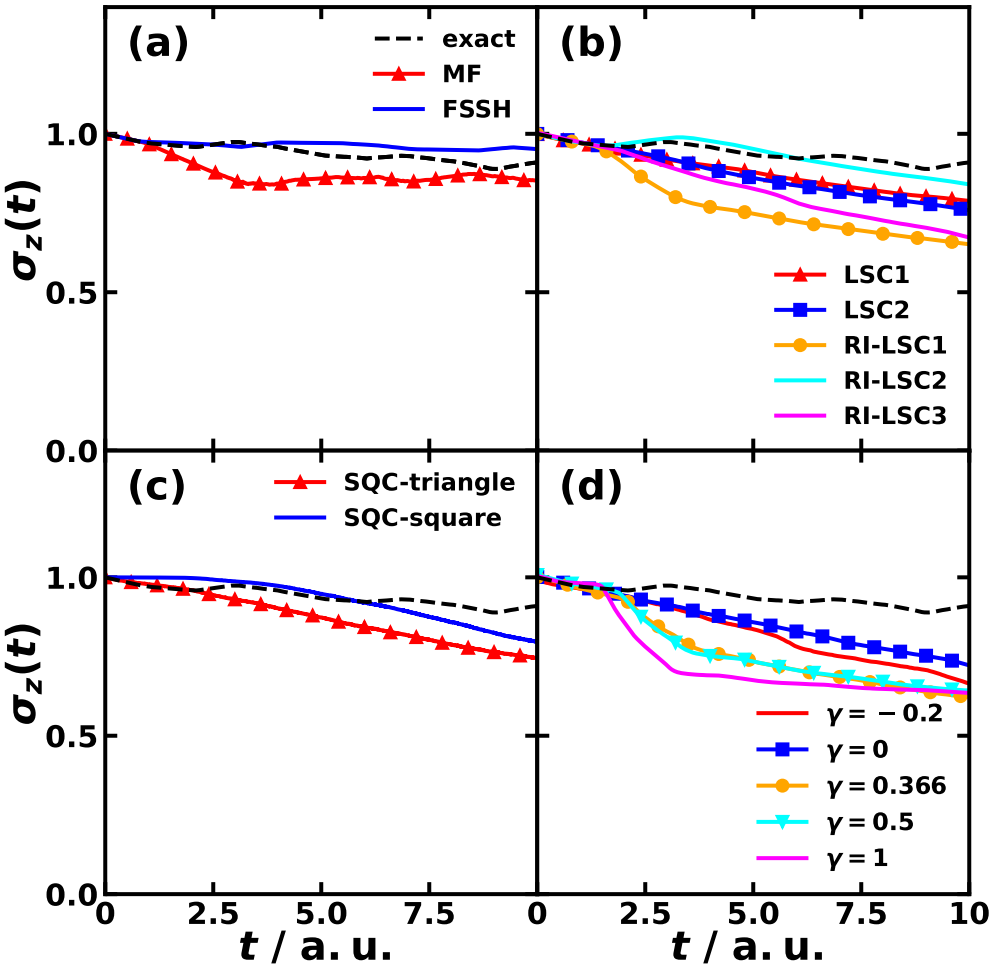

FIG. S23. Line cross parabola potentials are tested. In panel (a), mixed quantum-classical dynamics are benchmarked with the numerically exact results (black), in panel (b), LSC mapping dynamics are benchmarked, in panel (c), SQC dynamics are benchmarked, and in panel (d), SPM dynamics are benchmarked. The initial nuclear state is the vibrational eigenstate of $n = 30$ of the harmonic oscillator and electronic dynamics begins at the parabola state.

TABLE S5. Root mean square errors (RMSE) of various mapping dynamics compared to TT dynamics.

model	temperature	MF	FSSH	LSC1	LSC2	RI-LSC1	RI-LSC2	RI-LSC3	SQC-triangle	SQC-square	$\gamma = -0.2$	$\gamma = 0$	$\gamma = 0.366$	$\gamma = 0.5$	$\gamma = 1$
SBM #1	$0\,\Gamma/k_B$	0.166571	0.244687	0.129339	0.080415	0.067155	0.051691	0.053187	0.069639	0.075586	0.060589	0.051453	0.056260	0.065092	0.105582
SBM #1	$0.2\,\Gamma/k_B$	0.145825	0.218269	0.122279	0.078733	0.051108	0.047790	0.047629	0.059602	0.068567	0.053097	0.046509	0.050651	0.054732	0.072735
SBM #1	$2\,\Gamma/k_B$	0.102366	0.166393	0.103889	0.071602	0.029057	0.027235	0.027392	0.021924	0.027256	0.030982	0.029603	0.029483	0.031150	0.028487
SBM #2	$0\,\Gamma/k_B$	0.280288	0.441381	0.214542	0.203792	0.065685	0.036643	0.042255	0.058163	0.057842	0.045323	0.044018	0.059004	0.069931	0.104262
SBM #2	$0.2\,\Gamma/k_B$	0.282645	0.434463	0.210702	0.203897	0.043508	0.045269	0.047257	0.048278	0.050730	0.062937	0.052031	0.038937	0.044510	0.073719
SBM #3	$0\,\Gamma/k_B$	0.407437	0.335381	0.154380	0.327406	0.082397	0.070726	0.028276	0.099216	0.105122	0.020749	0.030056	0.066139	0.077146	0.145118
SBM #3	$0.2\,\Gamma/k_B$	0.403462	0.329057	0.152239	0.324600	0.077871	0.068344	0.025149	0.095010	0.099408	0.019976	0.024503	0.056288	0.076336	0.144168
SBM #3	$2\,\Gamma/k_B$	0.231354	0.150352	0.096465	0.180708	0.050490	0.024312	0.009188	0.033631	0.040786	0.016112	0.007802	0.026190	0.032556	0.098207
SBM #3	$10\,\Gamma/k_B$	0.052587	0.043898	0.011220	0.054313	0.042229	0.021069	0.020683	0.031186	0.037165	0.021954	0.022031	0.031239	0.038874	0.070664
SBM #4	$0\,\Gamma/k_B$	0.039322	0.104509	0.076803	0.022721	0.074733	0.025617	0.026321	0.060426	0.057490	0.016546	0.023789	0.064604	0.081536	0.129242
SBM #4	$0.2\,\Gamma/k_B$	0.040403	0.103035	0.076371	0.027156	0.074252	0.028697	0.029049	0.059523	0.058253	0.020214	0.028439	0.064569	0.078566	0.127517
SBM #5	0 K	0.192281	0.192658	0.172377	0.172973	0.046249	0.031479	0.020770	0.029430	0.051335	0.046682	0.021543	0.031592	0.048281	0.117798
SBM #5	300 K	0.169427	0.175205	0.099605	0.173699	0.140131	0.126386	0.122348	0.128920	0.137928	0.128250	0.124837	0.129509	0.133545	0.157401
SBM #6	0 K	0.345399	0.380052	0.316511	0.413412	0.329110	0.257277	0.036035	0.165108	0.140254	0.078688	0.020003	0.214799	0.329077	0.733039
SBM #6	300 K	0.187637	0.193284	0.182322	0.197099	0.209861	0.159396	0.147920	0.178913	0.187399	0.132855	0.142717	0.181572	0.200315	0.289628
SBM #7	0 K	0.188572	0.304953	0.221015	0.124617	0.110901	0.072412	0.066676	0.090709	0.086986	0.053758	0.065943	0.103319	0.117115	0.165956
SBM #7	300 K	0.149478	0.199312	0.024792	0.129056	0.068744	0.064666	0.065668	0.069048	0.072742	0.075335	0.067131	0.064890	0.064704	0.072351
SBM #8	0 K	0.311109	0.508929	0.256020	0.206398	0.069613	0.067776	0.063839	0.072482	0.068064	0.049677	0.068330	0.119624	0.119443	0.078209
SBM #8	300 K	0.091456	0.139666	0.064765	0.074239	0.036869	0.030173	0.029515	0.031300	0.036074	0.031673	0.029698	0.033111	0.036802	0.058307
SBM #9	$0\,\Gamma/k_B$	0.099903	0.125503	0.047681	0.042803	0.044461	0.044201	0.043230	0.052197	0.071051	0.045666	0.038944	0.044861	0.045967	0.048441
SBM #9	$0.2\,\Gamma/k_B$	0.078304	0.094115	0.042372	0.036261	0.039091	0.038112	0.039970	0.039861	0.061627	0.038513	0.035346	0.037886	0.040806	0.041128
SBM #9	$2\,\Gamma/k_B$	0.020471	0.475250	0.025719	0.015786	0.019593	0.020009	0.021286	0.020522	0.038954	0.019458	0.016356	0.017075	0.015870	0.019742
SBM #9	$10\,\Gamma/k_B$	0.011502	0.014886	0.020676	0.009217	0.011878	0.012119	0.011787	0.011933	0.027444	0.011465	0.011802	0.016590	0.011613	0.012545
Fulvene	0 K	0.161815	0.326893	0.046333	0.195356	0.033407	0.051680	0.261998	0.032235	0.034878	0.433400	0.213522	0.034120	0.070773	0.175249
Fulvene	300 K	0.163135	0.326777	0.044421	0.196735	0.033701	0.053426	0.260458	0.032433	0.034331	0.435539	0.215547	0.034078	0.072522	0.173803
BMA	0 K	0.033660	0.025581	0.006710	0.045110	0.003700	0.049061	0.042252	0.043634	0.031176	0.074459	0.041231	0.008613	0.017458	0.035590
BMA	300 K	0.034190	0.024552	0.003466	0.047075	0.004443	0.050180	0.045540	0.042600	0.031721	0.075691	0.049175	0.007747	0.018659	0.038575
MIA	0 K	0.022879	0.031240	0.046468	0.043701	0.039566	0.018239	0.045836	0.011570	0.038648	0.083748	0.045880	0.030251	0.057512	0.120289
MIA	300 K	0.044658	0.059730	0.078419	0.072716	0.063822	0.035509	0.058795	0.020758	0.034079	0.118337	0.066274	0.056898	0.093465	0.189011

TABLE S6. Computational cost for various model systems using different approximate dynamical methods. Computational time is in the units of core-hour with Intel Xeon Gold 6132 CPU with a base frequency of 2.6 GHz and turbo frequency of 3.7 GHz.

model	FSSH	MF	LSC	other mapping dynamics
SBM #1–4,9	0.10	0.81	80.5	8.1
SBM #5–8	0.01	1.0	8.2	1.0
Fullene	0.3	2.7	222	25.7
BMA	0.2	1.2	120	11.8
MIA	0.2	1.1	150	12.2
Retinal	0.05	0.4	35.2	4.5

TABLE S7. Computational cost for spin-boson model using TT-KSL (zero temperature) and TT-TFD (finite temperature) methods. The walltime for each propagation step (second/step) is measured using 28 cores in dual Intel Xeon Gold 6132 CPU with a base frequency of 2.6 GHz and turbo frequency of 3.7 GHz. Here, simulation parameters include the number of occupation number basis for each mode (# of basis), the TT-rank, and the time step (Δt). The total cost is measured in core-hour using the above CPU.

model	temperature	# of basis	TT-rank	Δt	walltime (second/step)	total steps	total cost (core-hour)
SBM #1	0	25	20	0.0036 $\hbar/\Gamma$	1.37	4200	44.8
SBM #1	2 Γ/k_B	25	80	0.05 $\hbar/\Gamma$	72.0	300	168
SBM #2	0	25	20	0.0036 $\hbar/\Gamma$	1.40	4200	45.8
SBM #2	0.2 Γ/k_B	25	20	0.0036 $\hbar/\Gamma$	3.62	4200	118
SBM #3	0	25	20	0.0036 $\hbar/\Gamma$	1.36	4200	44.3
SBM #3	10 Γ/k_B	25	90	0.00625 $\hbar/\Gamma$	100.	2400	1875
SBM #4	0	25	20	0.0036 $\hbar/\Gamma$	1.38	4200	45.1
SBM #4	0.2 Γ/k_B	25	20	0.0036 $\hbar/\Gamma$	3.39	4200	111
SBM #5	0	25	20	10 au	2.69	4200	87.8
SBM #5	300 K	25	150	10 au	324	4200	10575
SBM #6	0	25	20	10 au	2.04	4200	66.6
SBM #6	300 K	25	140	10 au	262	4200	8558
SBM #7	0	25	20	10 au	2.13	4200	69.6
SBM #7	300 K	25	150	10 au	291	4200	9494
SBM #8	0	25	20	10 au	1.98	4200	64.6
SBM #8	300 K	25	160	10 au	396	4200	12940
SBM #9	0	25	20	0.1 $\hbar/\Gamma$	1.52	150	1.78
SBM #9	10 Γ/k_B	25	20	0.1 $\hbar/\Gamma$	4.07	150	4.75

TABLE S8. Linearized semiclassical (LSC) mapping dynamics.

paper	year	method	model tested
Ref. 4	1970	VV-IVR	scattering
Ref. 5	1984	HK-IVR	–
Ref. 6	2002	HK-IVR	–
Ref. 7	2006	HK-IVR	–
Ref. 8	1997	SC-IVR	Tully
Ref. 9	1998	LSC-IVR†	SBM, Tully
Ref. 10	1998	LSC-IVR	SBM
Ref. 11	2001	LSC-IVR	PDM
Ref. 12	2008	PBME*	SBM
Ref. 13	2019	RI-LSC‡	SBM
Ref. 14	2020	RI-LSC‡	SBM, FBX, Tully
Ref. 15	2021	RI-LSC‡	SBM, MSH
Ref. 16	2022	RI-LSC‡	all-atom
Ref. 17	2022	RI-LSC‡	MSH, FMO
Ref. 18	2023	RI-LSC‡	MRC, FMO
Ref. 19	2023	RI-LSC‡	SBM, ANH

† LSC-IVR, linearized semiclassical initial value representation (referred to as LSC2)
∗ PBME, Poisson bracket mapping equation (referred to as LSC1)
‡ RI-LSC, resolution of identity linearized semiclassical dynamics; Here, $\phi_1\phi_1$, $\phi_1\phi_2$, and $\phi_2\phi_2$ of Ref. 14 are referred to as RI-LSC1, RI-LSC2, and RI-LSC3, respectively.
Abbreviation: VV-IVR, Van-Vleck initial value representation; HK-IVR, Herman-Kulk initial value representation; VV-IVR and HK-IVR are major semiclassical initial value representation (SC-IVR); SBM, spin-boson model; Tully, Tully's scattering models; FBX, Frenkel biexciton model; FMO, Fenna-Matthews-Olson complex model; PDM, Miller's photodissociation model; PCET, proton-coupled electron transfer model; ANH, 1-dimensional anharmonic model; MSH, multi-state harmonic model; MRC, multistate reaction coordinate model.

TABLE S9. Symmetrical quasiclassical (SQC) mapping dynamics.

paper	year	method	model tested
Ref. 20	2013	SQC-square	H+H_2 scattering
Ref. 21	2014	SQC-square	SBM and PCET
Ref. 22	2015	SQC spin-S mapping	SBM, Tully
Ref. 23	2015	SQC-square	SBM
Ref. 24	2016	SQC-triangle	SBM, Tully, FBX
Ref. 25	2016	SQC-square	FMO
Ref. 26	2016	SQC quantization	FBX
Ref. 27	2017	SQC adiabatic	SBM
Ref. 28	2019	SQC adjust-γ †	PDM, SBM
Ref. 29	2019	SQC-triangle	24-, 48-, and 96-state FMO
Ref. 14	2020	SQC-triangle	SBM, FBX, Tully
Ref. 15	2021	SQC-square,triangle	SBM, MSH
Ref. 16	2022	SQC-triangle	all-atom
Ref. 17	2022	SQC-square	MSH, FMO
Ref. 19	2023	SQC-triangle	SBM, ANH
Ref. 18	2023	SQC-triangle	MRC, FMO

†: Trajectory-based ZPE parameter adjustment to ensure the initial effective force is on the initial state.
Abbreviation: SBM, spin-boson model; Tully, Tully's scattering models; FBX, Frenkel biexciton model; FMO, Fenna-Matthews-Olson complex model; PDM, photodissociation model; PCET, proton-coupled electron transfer model; ANH, 1-dimensional anharmonic model; MSH, multi-state harmonic model; MRC, multistate reaction coordinate model.

TABLE S10. Classical mapping model (CMM) mapping dynamics.

paper	year	method	model tested
Ref. 30	2016	CMM (#1-6)	RM
Ref. 31	2017	CMM	RM
Ref. 32	2019	CMM	SBM
Ref. 33	2021	eCMM	SBM
Ref. 34	2021	eCMMcv	Tully, PDM, FMO, AIC
Ref. 35	2021	eCMM, eCMMcv	SBM, PDM, FMO, AIC, RM
Ref. 36	2022	wMM	SBM, Tully, FMO, AIC, LVC
Ref. 16	2022	eCMM	all-atom
Ref. 17	2022	eCMM	MSH, FMO
Ref. 18	2023	eCMM	MRC, FMO
Ref. 37	2024	NAF	SBM, FMO, PDM, AIC, LVC

Abbreviation: CMM, classical mapping model; eCMM, extended classical mapping model; eCMMcv, extended classical mapping model with commutator variables; NAF, nonadiabatic field; RM, resonant model; PDM, photodissociation model; AIC, atom-in-cavity model; LVC, linear vibronic coupling model; MSH, multi-state harmonic model; MRC, multistate reaction coordinate model.

TABLE S11. Spin mapping model (SPM) mapping dynamics.

paper	year	method	model tested
Ref. 38	2019	SPM	SBM
Ref. 39	2020	SPM	FMO
Ref. 40	2022	SPM	SBM
Ref. 41	2022	SPM	SBM, LVC, FMO
Ref. 16	2022	SPM	all-atom
Ref. 17	2022	SPM	MSH, FMO
Ref. 18	2023	SPM	MRC, FMO
Ref. 19	2023	SPM	SBM, ANH
Ref. 42	2023	SPM, MASH	SBM, Tully

Abbreviation: SPM, spin-mapping dynamics, referred to as spin-LSC in some papers; MASH, mapping approach to surface hopping; SBM, spin-boson model; Tully, Tully's scattering models; FMO, Fenna-Matthews-Olson complex model; LVC, linear vibronic coupling model; ANH, 1-dimensional anharmonic model; MSH, multi-state harmonic model; MRC, multistate reaction coordinate model.

REFERENCES

[1] N. Makri, "The Linear Response Approximation and Its Lowest Order Corrections: An Influence Functional Approach," J. Phys. Chem. B **103**, 2823–2829 (1999).
[2] A. F. Izmaylov, D. Mendive Tapia, M. J. Bearpark, M. A. Robb, J. C. Tully, and M. J. Frisch, "Nonequilibrium Fermi Golden Rule for Electronic Transitions Through Conical Intersections," J. Chem. Phys. **135**, 234106 (2011).
[3] M. D. Newton and N. Sutin, "Electron Transfer Reactions in Condensed Phases." Annu. Rev. Phys. Chem. **35**, 437–480 (1984).
[4] W. H. Miller, "Semiclassical Theory of Atom-Diatom Collisions: Path Integrals and the Classical S Matrix," J. Chem. Phys. **53**, 1949–12 (1970).
[5] M. F. Herman and E. Kluk, "A Semiclasical Justification for the Use of Non-spreading Wavepackets in Dynamics Calculations," Chem. Phys. **91**, 27–34 (1984).
[6] W. H. Miller, "An Alternate Derivation of the Herman-Kluk (Coherent State) Semiclassical Initial Value Representation of the Time Evolution Operator," Mol. Phys. **100**, 397–400 (2002).
[7] K. G. Kay, "The Herman-Kluk Approximation: Derivation and Semiclassical Corrections," Chem. Phys. **322**, 3–12 (2006).
[8] X. Sun and W. H. Miller, "Semiclassical Initial Value Representation for Electronically Nonadiabatic Molecular Dynamics," J. Chem. Phys. **106**, 6346–6353 (1997).
[9] X. Sun, H. Wang, and W. H. Miller, "Semiclassical Theory of Electronically Nonadiabatic Dynamics: Results of a Linearized Approximation to the Initial Value Representation," J. Chem. Phys. **109**, 7064–7074 (1998).
[10] H. Wang, X. Sun, and W. H. Miller, "Semiclassical Approximations for the Calculation of Thermal Rate Constants for Chemical Reactions in Complex Molecular Systems," J. Chem. Phys. **108**, 9726–9736 (1998).
[11] E. A. Coronado, J. Xing, and W. H. Miller, "Ultrafast Non-Adiabatic Dynamics of Systems with Multiple Surface Crossings: A Test of the Meyer-Miller Hamiltonian with Semiclassical Initial Value Representation Methods," Chem. Phys. Lett. **349**, 521–529 (2001).
[12] H. Kim, A. Nassimi, and R. Kapral, "Quantum-Classical Liouville Dynamics in the Mapping Basis," J. Chem. Phys. **129**, 084102 (2008).
[13] M. A. C. Saller, A. Kelly, and J. O. Richardson, "On the Identity of the Identity Operator in Nonadiabatic Linearized Semiclassical Dynamics," J. Chem. Phys. **150**, 071101 (2019).
[14] X. Gao, M. A. C. Saller, Y. Liu, A. Kelly, J. O. Richardson, and E. Geva, "Benchmarking Quasiclassical Mapping Hamiltonian Methods for Simulating Electronically Nonadiabatic Molecular Dynamics." J. Chem. Theory Comput. **16**, 2883–2895 (2020).
[15] Z. Hu, D. Brian, and X. Sun, "Multi-State Harmonic Models with Globally Shared Bath for Nonadiabatic Dynamics in the Condensed Phase," J. Chem. Phys. **155**, 124105 (2021).
[16] Z. Hu and X. Sun, "All-Atom Nonadiabatic Semiclassical Mapping Dynamics for Photoinduced Charge Transfer of Organic Photovoltaic Molecules in Explicit Solvents," J. Chem. Theory Comput. **18**, 5819–5836 (2022).
[17] Z. Hu, Z. Liu, and X. Sun, "Effects of Heterogeneous Protein Environment on Excitation Energy Transfer Dynamics in the Fenna-Matthews-Olson Complex," J. Phys. Chem. B **126**, 9271–9287 (2022).
[18] Z. Liu, H. Hu, and X. Sun, "Multistate Reaction Coordinate Model for Charge and Energy Transfer Dynamics in the Condensed Phase," J. Chem. Theory Comput. **19**, 7151–7170 (2023).
[19] G. Amati, J. R. Mannouch, and J. O. Richardson, "Detailed Balance in Mixed Quantum–Classical Mapping Approaches," J. Chem. Phys. **159**, 214114 (2023).
[20] S. J. Cotton and W. H. Miller, "Symmetrical Windowing for Quantum States in Quasi-Classical Trajectory Simulations," J. Phys. Chem. A **117**, 7190–7194 (2013).
[21] S. J. Cotton, K. Igumenshchev, and W. H. Miller, "Symmetrical Windowing for Quantum States in Quasi-Classical Trajectory Simulations: Application to Electron Transfer," J. Chem. Phys. **141**, 084104 (2014).
[22] S. J. Cotton and W. H. Miller, "A Symmetrical Quasi-Classical Spin-Mapping Model for the Electronic Degrees of Freedom in Non-Adiabatic Processes," J. Phys. Chem. A **119**, 12138–12145 (2015).
[23] W. H. Miller and S. J. Cotton, "Communication: Note on Detailed Balance in Symmetrical Quasi-Classical Models for Electronically Non-Adiabatic Dynamics," J. Chem. Phys. **142**, 131103 (2015).
[24] S. J. Cotton and W. H. Miller, "A New Symmetrical Quasi-Classical Model for Electronically Non-Adiabatic Processes: Application to the Case of Weak Non-Adiabatic Coupling," J. Chem. Phys. **145**, 144108 (2016).
[25] S. J. Cotton and W. H. Miller, "The Symmetrical Quasi-Classical Model for Electronically Non-Adiabatic Processes Applied to Energy Transfer Dynamics in Site-Exciton Models of Light-Harvesting Complexes," J. Chem. Theory Comput. **12**, 983–991 (2016).
[26] W. H. Miller and S. J. Cotton, "Communication: Wigner Functions in Action-Angle Variables, Bohr-Sommerfeld Quantization, the Heisenberg Correspondence Principle, and a Aymmetrical Quasi-Classical Approach to the Full Electronic Density Matrix," J. Chem. Phys. **145**, 081102 (2016).
[27] S. J. Cotton, R. Liang, and W. H. Miller, "On the Adiabatic Representation of Meyer-Miller Electronic-Nuclear Dynamics," J. Chem. Phys. **147**, 064112 (2017).
[28] S. J. Cotton and W. H. Miller, "Trajectory-Adjusted Electronic Zero Point Energy in Classical Meyer-Miller Vibronic Dynamics: Symmetrical Quasiclassical Application to Photodissociation," J. Chem. Phys. **150**, 194110 (2019).
[29] S. J. Cotton and W. H. Miller, "A Symmetrical Quasi-Classical Windowing Model for the Molecular Dynamics Treatment of Non-Adiabatic Processes Involving Many Electronic States," J. Chem. Phys. **150**, 104101 (2019).
[30] J. Liu, "A Unified Theoretical Framework for Mapping Models for the Multi-State Hamiltonian," J. Chem. Phys. **145**, 204105 (2016).
[31] J. Liu, "Isomorphism between the Multi-State Hamiltonian and the Second-Quantized Many-Electron Hamiltonian with Only 1-Electron Interactions," J. Chem. Phys. **146**, 024110 (2017).
[32] X. He and J. Liu, "A New Perspective for Nonadiabatic Dynamics with Phase Space Mapping Models," J. Chem. Phys. **151**, 024105 (2019).
[33] X. He, Z. Gong, B. Wu, and J. Liu, "Negative Zero-Point-Energy Parameter in the Meyer-Miller Mapping Model for Nonadiabatic Dynamics," J. Phys. Chem. Lett. **12**, 2496–2501 (2021).
[34] X. He, B. Wu, Z. Gong, and J. Liu, "Commutator Matrix in Phase Space Mapping Models for Nonadiabatic Quantum Dynamics," J. Phys. Chem. A **125**, 6845–6863 (2021).
[35] J. Liu, X. He, and B. Wu, "Unified Formulation of Phase Space Mapping Approaches for Nonadiabatic Quantum Dynamics," Acc. Chem. Res. **54**, 4215–4228 (2021).
[36] X. He, B. Wu, Y. Shang, B. Li, X. Cheng, and J. Liu, "New Phase Space Formulations and Quantum Dynamics Approaches," WIREs Comput. Mol. Sci. (2022), 10.1002/wcms.1619.
[37] B. Wu, X. He, and J. Liu, "Nonadiabatic Field on Quantum Phase Space: A Century after Ehrenfest," J. Phys. Chem. Lett. **15**, 644–658 (2024).
[38] J. E. Runeson and J. O. Richardson, "Spin-Mapping Approach for Nonadiabatic Molecular Dynamics," J. Chem. Phys. **151**, 044119 (2019).

[39] J. E. Runeson and J. O. Richardson, "Generalized Spin Mapping for Quantum-Classical Dynamics," J. Chem. Phys. **152**, 084110 (2020).
[40] G. Amati, M. A. C. Saller, A. Kelly, and J. O. Richardson, "Quasiclassical Approaches to the Generalized Quantum Master Equation," J. Chem. Phys. **157**, 234103 (2022).
[41] J. E. Runeson, J. R. Mannouch, G. Amati, M. R. Fiechter, and J. O. Richardson, "Spin-Mapping Methods for Simulating Ultrafast Nonadiabatic Dynamics," Chimia **76**, 582 (2022).
[42] J. R. Mannouch and J. O. Richardson, "A Mapping Approach to Surface Hopping," J. Chem. Phys. **158**, 104111 (2023).